POLITECNICO DI TORINO

MASTER's Degree in Biomedical Engineering

MASTER's Degree Thesis

Low-cost Neuronal Network Electronic Readout Circuit for Micro-Graphitic Diamond Multi-Electrode Arrays

Supervisors
Prof. Eng. Danilo DEMARCHI
Eng. Alessandro SANGINARIO

Candidate
Marco BOSCHERINI

Academic year 2021-2022

Abstract

The development of advanced microelectrode array (MEA) technology interfaced with low-noise high-gain conditioning circuits is crucial for evaluating the electrophysiological properties of neurons. The simultaneous and parallel access to the activity of a large population of neurons within a network aids the investigation of information processing and learning aspects of neural behavior. This project presents an early-stage design phase of a low-cost electronic readout circuit interfaced with Micro-Graphitic Diamond Multi-Electrode Arrays (µG-D-MEAs), for the real-time monitoring of the activity of cultured neurons in a potentiometric configuration. The developed Analog Front-End (AFE) is a single-channel device consisting of multiple amplifying and filtering stages. The input signal's amplitude is of the order of tens of µV, thus the AFE has been designed to have a high gain and match the very low noise requirements imposed by the neuronal cell cultures. The most critical amplifying stage is based on the LMP7721 integrated circuit (a precision operational amplifier) which exhibits an ultra-low input bias current of 3 fA and voltage noise of 6.5 $nV/\sqrt{Hz}$. The AFE has been assessed by simulating a neuron spike shape by using the Agilent B2912A Precision Source/Measure Unit. It exhibited good performance when compared with a real neuron spike recorded with the commercial MEA1060-Inv-BC from Multichannel Systems, resulting in a <10 μV_{RMS} background noise. Finally, dopaminergic neurons from substantia nigra (SN) have been used both as a test bench for the AFE and for scientific research. The device has been coupled with the cell culture inside an incubator with a controlled temperature of 37°C and the signals have been acquired from different channels. The recordings showed the presence of the neuron spikes with a 1 to 10 Hz mean firing frequency and a -22 to -37 µV average peak amplitude, depending on the channel considered. The noise level varied depending on the selected channel and, in the worst case, it proved to be smaller than 10 μV_{RMS}. The results have been compared with the commercial device's acquisitions, showing similar performances. The outcomes demonstrated that this project is ideal to be the first step of a wider plan. Looking to the future, further developments of the device may lead to extending the number of recording channels and to integrating the amperometric configuration with the potentiometric one, for a dual simultaneous and parallel mode.

Acknowledgements

I wish to dedicate a few words to all the people who have accompanied me through this path during the last years. A special regard goes to my family, who have supported me unconditionally both in the difficult and in the most bright moments. I want to express gratitude to my thesis supervisors who gave me the opportunity to join a great working environment and guided me in the realisation of this project and in my professional growth. Finally, a fond thought goes to everyone who has shared this part of life with me. Thank you, I hope to be able to give back to you everything you gave to me.

Desidero spendere alcune parole per tutte le persone che mi hanno accompagnato in questo percorso durante gli ultimi anni. Una considerazione speciale va alla mia famiglia, che mi ha supportato incondizionamente sia nei momenti più difficili che in quelli più gioiosi. Voglio esprimere la mia gratitudine per i miei supervisori di tesi, i quali mi hanno dato l'opportunità di far parte di un fantastico ambiente di lavoro e che mi hanno guidato nella realizzazione di questo progetto e nella mia crescita professionale. In fine, un pensiero va a tutti coloro che hanno condiviso con me questo periodo di vita. Grazie, spero di riuscire a ridarvi indietro tutto ciò che voi avete dato a me.

Marco.

Contents

List of Tables

List of Figures

Acronyms

ADC	*Analog-to-Digital Converter*
AFE	*Analog Front-End*
AP	*Action Potential*
BJT	*Bipolar Junction Transistor*
CE	*Counter Electrode*
CMOS	*Complementary Metal-Oxide Semiconductor*
CNS	*Central Nervous System*
DAC	*Digital-to-Analog Converter*
DC	*Direct Current*
DET	*Dipartimento di Elettronica e Telecomunicazioni*
DIV	*Days-In-Vitro*
D-MEA	*Diamond-based Multi-Electrode Array*
EPSP	*Excitatory PostSynaptic Potential*
FET	*Field-Effect Transistor*
FP	*Field Potential*
GABA	*Gamma-Aminobutyric Acid*
GPCR	*G-Protein-Coupled Receptor*
GPIO	*General Purpose Input/Output*
GUI	*Graphical User-Interface*
HDMEA	*High-Density Multi-Electrode Array*
HPF	*High-Pass Filter*
IIR	*Infinite Impulse Response*
IOA	*Inverting Operational Amplifier*
IPSP	*World Health Organization*
LED	*Light-Emitting Diode*
LPF	*Low-Pass Filter*
LVR	*Linear Voltage Regulator*
MCU	*Micro-Controller Unit*
MEA	*Multi-Electrode Array*
MP	*Membrane Potential*

NIOA	*Non-Inverting Operational Amplifier*
NISC	*Non-Inverting Summing Circuit*
OA	*Operational Amplifier*
PC	*Personal Computer*
PCB	*Printed Circuit Board*
PLA	*PolyLactic Acid*
PNS	*Peripheral Nervous System*
PSD	*Power Spectral Density*
RE	*Reference Electrode*
RMS	*Root-Mean-Square*
SMU	*Source/Measure Unit*
SN	*Substantia Nigra*
SNR	*Signal-to-Noise Ratio*
TIA	*Transimpedance Amplifier*
USB	*Universal Serial Bus*
USB-OTG	*Universal Serial Bus On-The-Go*
WE	*Working Electrode*
WHO	*World Health Organization*

1 Introduction

Since ancient times, understanding the brain has been one of the main goals for humanity, due to its extremely high complexity and the wide range of performable functions which this organ can execute. The progress achieved to gather knowledge in this complicated field has been considerable, with a huge acceleration in the last decades. There are still a multitude of aspects "in the dark" though and consequently still a great potential to figure out in the future. For this purpose, neuroscience plays a key role.

Neuroscience is a multidisciplinary science, with the aim of studying the nervous system and its functions, in addition to finding cures for many disorders and pathologies. The World Health Organization (WHO) stated in a report written in 2007 that up to 1 billion people in the world suffer from mental disorders and neurological pathologies [1], such as epilepsy, Parkinson's disease and Alzheimer's. The studies also estimated that nearly 7 million people's deaths are directly correlated with these pathologies. These numbers are easily large enough to understand how important it is to invest a great deal in basic research and in the development of new techniques and treatments.

To this end, one of the most interesting and trendy techniques is surely cell culture, which enables one to grow and analyse different types of cells under controlled conditions. This method shows many advantages and a great future perspective, although there are few vital issues which must be solved in the next years to be a stronger alternative for *in vivo* experimentation and further improvement of the basic scientific research capacity. The last few decades have seen a quick and constant increment in the use of mammalian cell cultures in laboratories and of the demand of the corresponding products. Some estimations [2] reveal how in the next years the trend is going to rise even more, as shown in **Figure 1**.

Nowadays cell cultures are increasingly coupled with multi-electrode arrays (MEAs). This technology allows the recording and stimulation of electrical activity in excitable cells, such as neurons, muscle cells and endocrine cells. The main advantage is the capability to perform extracellular recordings and stimulate excitable cells at multiple sites simultaneously [3].

1.1 Aim of the project

This thesis dissertation presents the preliminary design phase of a versatile and innovative low-cost electronic device for interfacing neuronal cell cultures based on novel diamond-based MEAs. For this early-stage part of the

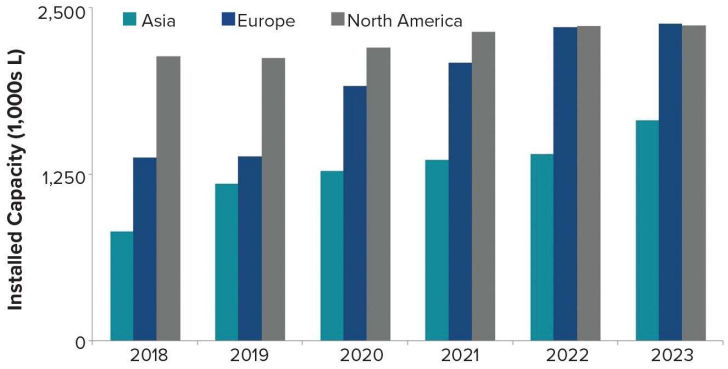

Figure 1: Geographic distribution of manufacturing capacity for products based on mammalian-cell culture [2]

project, the aim is to develop a low-noise single-channel readout circuit for monitoring the electrical activity of cultured neurons.

However, this is just the first stage of an ambitious plan. Further steps involve designing a 60-channel precision electronic system able to perform parallel tasks, including simultaneous recordings in different modalities and neuron electrical stimulation.

The project has been implemented in collaboration with the University of Torino (Italy), in particular with the Department of Drug and Science Technology and the Department of Physics.

Moreover, a rewarding cooperation with researchers from the Molecular Biotechnology Center of the University of Torino led to the conduction of a different type of experiment, interfacing the designed device with interdigitated electrodes usually used for purposes other than potentiometric recordings.

1.2 Physiology fundamentals - Nervous System

Figure 2: Colored representation of nervous system [4].

The nervous system is the main controlling, regulatory, and communicating system in the body and it is responsible for maintaining stability in the internal environment of living biological systems (homeostasis). It coordinates different body organs and systems to execute voluntary and involuntary functions [5].

The nervous system is constituted by the central nervous system (CNS) and the peripheral nervous system (PNS). The CNS is formed of the brain and the spinal cord. Its main function is to receive and elaborate on the information coming from the whole body and, eventually, to execute an action sending the appropriate instructions to the organs of interest. PNS, on the other hand, consists of cells with the purpose of transmitting signals from organs to the SNC (afferent component) and vice versa (efferent component).

Neurons and glial cells form the nervous system and play different roles. Neurons are excitable cells that communicate with each other via electrical pulses, whereas glial cells provide structural and metabolic support to neurons [6].

1.2.1 Neurons

The neuron is an electrically excitable cell, responsible for carrying information to other cells throughout the body via electrical and chemical signals. Their main role is to control and coordinate all of the body's vital activities and functions [7]. In a study, reported in 2009 [8], a group of scientists estimated that there are approximately 86 billion neurons in the whole hu-

man brain, each with thousands of synapses (i.e., connections with other neurons)[9]. These numbers show the remarkable complexity of the communication network in the CNS.

The neuron structure, in most of the cases, can be represented by three parts (as shown in **Figure 3**): cell body (soma), dendrites and axon. The

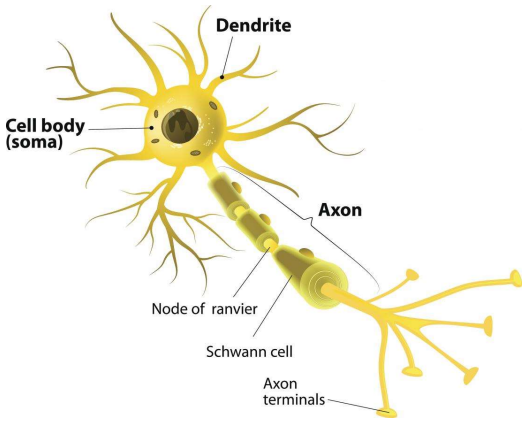

Figure 3: Simplified representation of a neuron [7].

soma contains the neuron nucleus and it is responsible for protein synthesis and cellular metabolism. Dendrites are thin filaments that branch out from the cell body and receive information from other neurons. The axon is a relatively long projection attached to the soma, which carries signals from the neuron core and sends them to other cells via the axon terminals. Axons are often surrounded by a myelin sheath that insulates them and increases the rate at which electrical pulses travel [6][7].

The whole neuron has several ion channels which determine the electrical and chemical properties of the membrane. The channels can be either open or closed and some can change their conformation based on the occurrence of specific events. The ions' electrochemical status determines the value of the membrane potential (MP), that is the potential difference between the internal and the external part of the cell. At rest (i.e., no signal received or transmitted), the MP is generally -70 mV due to the concentration and electrical properties of ions in that specific condition.

When a graded potential reaches the threshold, an action potential (AP) is generated. Voltage-gated Na^+ channels open and a positive feedback occurs causing a rapid influx of Na^+ down its concentration gradient. The MP, therefore, increases due to the positive charges of the sodium ions en-

tering in the cell (depolarization). When the MP is about to a positive peak value, Na^+ channels begin to close while K^+ channels open and the K^+ ions rush out. As soon as the threshold has been crossed again, voltage-gates K^+ channels start closing, slowing down the ions' flux. Before returning to a rest condition, a hyerpolarization occurs owing to a still increased K^+ membrane permeability, compared to the Na^+ (**Figure 4**).

The 'all-or-none' event nature makes the AP propagate along the whole axon without attenuation [11]. Thanks to the refractory periods, affecting the axon's region after the AP has passed, the signal ideally travels in a unique direction: from the soma to the axon terminals [6].

When an axon region depolarizes enough to generate an AP, the inside becomes positive while the outside gets negative, unlike the adjacent areas (**Figure 5a**). Thus, the positive charges in the inner part move towards the

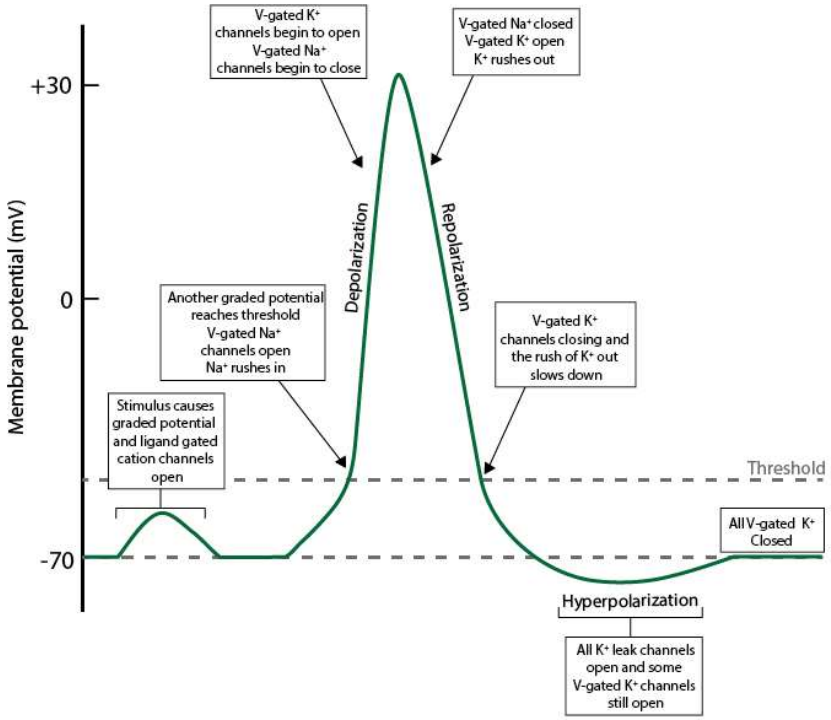

Figure 4: Typical shape of an action potential in relation to the opening and the closure of sodium (Na^+) and potassium (K^+) ion channels [10].

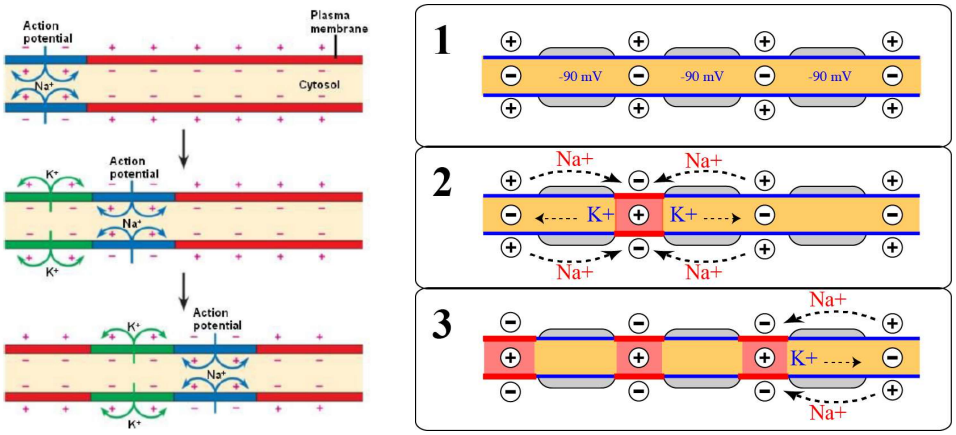

(a) Unmyelinated axon [12]. **(b)** Myelinated axon [13].

Figure 5: Simplified propagation mechanisms in case of (a) unmyelinated axons and (b) myelinated axons.

non-depolarized negative neighboring sides (due to electrostatic attraction) and vice versa regarding the external. That causes a depolarization in the new site and a re-polarization in the old one (which enters in a refractory status).

Processing the information quickly is critical for the brain to properly execute tasks, thus the speed of AP propagation is a particularly important feature. This is greatly increased by the presence of the myelin sheath and nodes of Ranvier (the coating interruptions) [11]. This propagation modality is called 'saltatory conduction' (**Figure 5b**). The myelin coating creates a great resistance to the ions flow and the nodes of Ranvier are the only spots where voltage-gated ion channels are located. Hence, here's the only region where membrane depolarization can occur. While in the normal AP propagation the neighborhood is adjacent to the depolarized zone, in the myelinated axons the distance between two nodes of Ranvier is higher. This means that in the latter the 'steps' the AP has to do are greater than in the former and consequently an increased propagation speed.

1.2.2 Synapses

Synapses are cellular regions where neurons functionally interact to each other. It's possible to classify two main modalities of synaptic transmission, i.e., electrical and chemical. Some studies say to not exclude the possi-

bility that neurons can communicate by other methods as well, such as volume transmission (the capability to excite or inhibit target cells due to the diffusion of neurotransmitters through the extracellular space) and the generation of electrical fields [14].

Electrical synapses allow the signal transmission between neurons via clusters of inter-cellular channels (gap junctions). The communication is quick, usually bidirectional and can be either excitatory or inhibitory (**Figure 6a**).

Chemical synapses are the most numerous and, probably, sophisticated neuronal connection in brain (**Figure 6b**). The signal transmission takes place owing to the activation of neurotransmitters, that are messenger molecules secreted by the 'presynaptic neuron' to affect a 'postsynaptic neuron'. When an AP depolarizes the axon terminal membrane, several voltage-gated Ca2+ channels open creating an inflow of calcium ions. These trigger the release of synaptic vesicles full of a specific neurotransmitter, in the small space between the two neurons, called synaptic cleft. The neurotransmitter molecules diffuse across the synapse to bind to specific postsynaptic membrane receptors. The neurotransmitter-receptors interaction leads to the opening of ion channels in the membrane, which modify the membrane potential. Chemical synapses can be either excitatory or inhibitory. The excitatory synapse causes a depolarization of the postsynaptic neuron's MP,

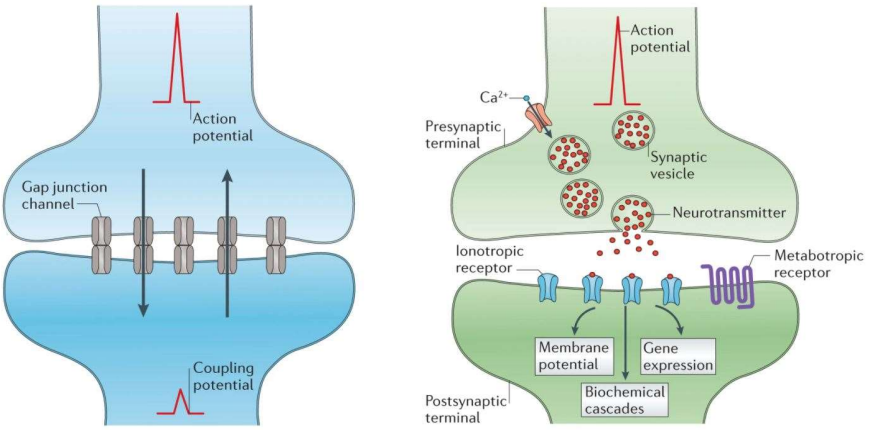

(a) Electrical synapse. **(b)** Chemical synapse.

Figure 6: Simplified representation of an electric synapse **(a)**, where the ion flux through the gap junctions determines the communication, and a more sophisticated chemical synapse **(b)**, in which the signal transmission is mediated by neurotransmitters [14].

named excitatory postsynaptic potential (EPSP), whereas an inhibitory synapse produces a hyper-polarization, known as inhibitory postsynaptic potential (IPSP). What matters to generate an AP in the communicating neuron is not the single postsynaptic potential. Indeed, there's never a unitary input for a neuron, but always a large number (up to thousands). The inputs sum spatially and temporally to each other and if the overall MP reaches the threshold, the AP sets off [6].

1.2.3 Neurotransmitters

Neurotransmitters are chemical substances that carry information from neurons to cells, such as other neurons, muscles, or glands. Several types of neurotransmitters exist, with different receptors and mechanisms for decoding their information content. The study of these molecules and their processes is critical in order to develop therapeutic drugs meant to treat neurological disorders, considering their key role in the brain.

The two main molecular structures found which work as receptors for neurotransmitters are ligand-gated channels (ionotropic) and G protein-coupled receptors (GPCRs) (**Figure 7**). Ionotropic receptors are directly connected to ion channels: as soon as the neurotransmitter binds with one of these structures, the channel opens, determining the flow of the specific ion. In ligand-gated channels the response is very quick, as well as the depolarization of the postsynaptic membrane in that site. GPCRs are indirectly connected to ion channels. The bond between the receptor and the neurotransmitter activates the G-protein, responsible to further generate the opening of the ion channel and the consequent membrane depolarization. This is a slow-response mechanism [15][6].

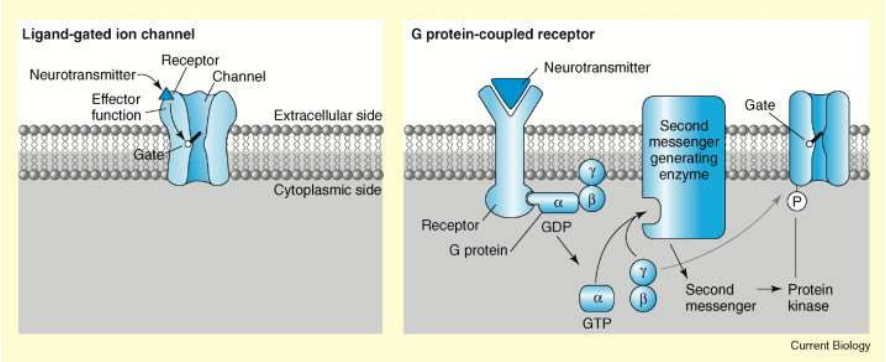

Figure 7: Neurotransmitter receptors [15].

The most common neurotransmitter in the nervous system is acetylcholine, used, for instance, in the neuromuscular junction. Once synthesized it's stored in vesicles until its release after a depolarization. Acetylcholine binds to cholinergic receptors, such as nicotinic (ionotropic) and muscarinic (GPCRs) receptors located in the postsynaptic membrane.

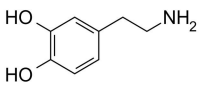

Figure 8: Dopamine chemical structure.

Dopamine plays a fundamental role in many vital functions, as well as in some neurological diseases. This neurotransmitter is stored in vesicles and released after an AP (quantal release). It can bind either to GPCRs postsynaptic receptors or GPCRs presynaptic receptors and can have either an excitatory or inhibitory potential [16][17].

1.2.4 Dopaminergic Neurons and Substantia Nigra

Dopaminergic neurons constitute the source of dopamine in the mammalian central nervous system [18]. They have been found mainly in mid-brain nuclei and they project to several fore-brain structures. These neurons are involved in numerous functions, such as control of movement, control of emotions, cognition, reward-related behavior, memory and so on. Hence, a dysfunction of them causes a wide range of brain disorders, including Parkinson's disease, schizophrenia, depression, addiction to some drugs, etc.

Dopaminergic neurons normally fire at relatively low frequencies (at around 5Hz) and occasionally they burst at higher frequencies. The magnitude of these burst firing depends on the type of stimulus the subject is exposed to: for instance, it's been proved in rats that dopaminergic neurons are inhibited in case of averse stimuli [19].

Dopaminergic neurons are not homogeneous in the mid-brain, in terms of functionality, physiology, projection patterns and susceptibility to diseases. They are normally divided in three sub-types: A8 (located in retrorubral field), A9 (substantia nigra pars compacta) and A10 (ventral tegmental area). [20].

The substantia nigra is a large pigmented group of neurons located in the midbrain and considered as a part of the basal nuclei. Among the several functions that the CNS plays, reward, addiction and movement are probably the most important ones [21] [22].

The substantia nigra is formed by two portions: the pars compacta and the pars reticulata. Individually they play different roles but, when working together, they contribute to the correct control of movement, reward-

seeking, learning and addiction.

The pars compacta contain the dark pigment neuromelanin, which gives the specific colour to the structure. Moreover, the pars compacta contains dopaminergic neurons (from the A9 group), which synthesize the correspondent neurotransmitter. These neurons constitute the nigrostriatal pathway, which connects the substantia nigra compacta to the corpus striatum: here the dopamine is released. The nigrostriatal pathway cells contain two different receptors for the dopamine neurotransmitter: excitatory receptors (D1) and inhibitory (D2). The main function of these structures is to indirectly regulate the motor control, by the mediation of the striatum.

The pars reticulata derives from the caudate and putamen nucleus of the striatum, as well. Its neurons project mainly to the thalamus and to a tiny part of the superior colliculus. Cells of pars reticulata produce an other neurotransmitter, GABA (gamma-aminobutyric acid), which plays an inhibitory activity on the thalamus and on the pars compacta. When the GABA joins its receptors, it causes the inhibition of the movement and the production of dopamine.

Substantia nigra neurons are the principal source of dopamine in the brain. Their degeneration determines the development of Parkinson's disease. Current treatments for Parkinson's disease are mostly based on the compensation of the progressive loss of striatal dopamine by administrating its precursor L-DOPA. This can cross through blood-brain barrier and alleviate Parkinson's symptoms. Other therapies include the deep brain stimulation, neuroablative surgery and gene therapy[23].

However, a real cure does not exist yet and the research on substantia nigra neurons (as cell cultures or tissue slices) results fundamental.

1.3 Cell Culture

Cell culture is a prominent technique for basic scientific research and several *in vitro* clinical trials, based on the growth of animal-based or plant-based cells in an artificial environment, under physiological conditions [24]. Animal cell cultures, for instance, have been used in numerous applications, including the study of the interaction of drugs (or other chemicals) with cells.

The great potential of this technology is determined by multiple factors. The consistency and reproducibility of the results are two of the main advantages of cell cultures, thanks to the accurately controlled physiological conditions of the physio-chemical environment in the cultured system.

Figure 9: Cell cultures

Furthermore, it's possible to perform several tasks with cells *in vitro*, such as electrical stimulation and measurement, cytotoxicity studies, or imaging techniques, otherwise more complicated to perform (or in many cases not possible) *in vivo*. Another considerable advantage is the possibility to generate homogeneous and highly pure populations of differentiated cells [25]. Finally, an important ethical aspect must be considered: further use of these techniques can lead to a significant reduction in the number of animals used in scientific experiments, with evident social and environmental benefits.

Nevertheless, there is also criticism regarding cell culture, regarding the high risk of chemical and microbial contamination (e.g., bacteria, viruses, and fungi), the lack of a provided complex environment wherein the cells may not be able to survive. Therefore, the effort that must be applied to obtain a relatively low number of cells is higher. These are just a few of multiple issues surrounding cell culture that scientists are working to overcome [26].

In primary cultures, cells are obtained directly from tissues. This technique represents one of the bests experimental models for *in vitro* studies. The growth rate is usually low and they are more heterogeneous than other types of cultures. They are also more representative of the original tissue and conserve expressive characteristics [27].

Secondary cultures are formed by a passaging (or sub-culturing) procedure, wherein the medium is removed and the cells are transferred into a fresh growth medium enabling the further propagation of the cells. This type of culture is long-lasting and is useful for obtaining a large population

of cells. However, after a certain period of time they tend to differentiate and generate anomalous cells.

1.4 Electrophysiological Methods

Electrophysiological methods are useful techniques to study the electrical activity of excitable cells, such as neurons. It is possible to classify them depending on the scale on which they are considered:

- Intracellular recordings
- Extracellular recordings

Intracellular recordings aim to precisely measure a single cell's electrical activity by directly inserting sharp, or patch microelectrodes into the cell membrane. The strength of these systems is in their ability to readout the entire dynamic of a neuron potential, including sub-threshold signals, accurately and with no distortion over time. However, the mechanical and biophysical instabilities make the recording session extremely limited and complicated [28].

Extracellular recordings use substrate-integrated multi-electrode arrays to readout the electrical activity of neuron networks. These methods permit very simple simultaneous acquisitions of large populations of cells for a long time (days/months), without damaging the membranes. Nevertheless, the recording of a high-number of action potentials widely attenuates and temporally filters the signal. Moreover, the study of sub-threshold membrane potentials becomes impossible [28].

A simplified representation of the interface between an electrode and a neuron is illustrated in **Figure 7**. The electrode immersed in electrolyte can be modelled as a resistance in parallel with a capacitance ($R_e \parallel C_e$). Both the neuron's membranes, i.e. the junctional and the non-junctional, can also be simplified as the parallel between a resistance and a capacitance, ($R_j \parallel C_j$ and $R_{nj} \parallel C_{nj}$, respectively). The solution in between the electrode and the neuron generates a conduction resistance (R_{seal}), which varies depending on the electrolyte's characteristics and influences the current flow across the electrode [29].

The recorded signal, commonly called field potential (FP), is generated by APs, but it undergoes significant attenuation and distortion. The coupling coefficient (the ratio between the maximal FP in response to the AP peak) depends on the frequency of APs, the electrode impedance, R_{seal} and the other parameters seen in the model above.

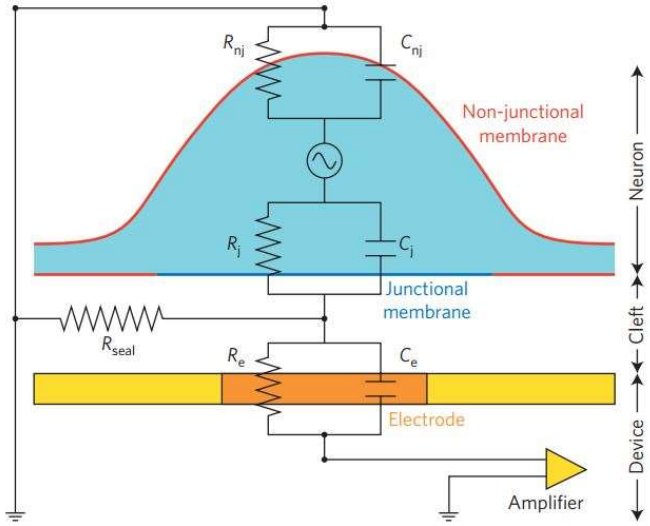

Figure 10: Simplified model of the interface between a substrate-integrated electrode (orange) and a neuron (blue). The electrode is coupled to an amplifier. The space between the neuron membrane and the electrode surface is the cleft. The neuron surface has been divided into a junctional membrane, facing the electrode, and a non-junctional membrane, facing the substrate (yellow) and the solution. AP propagation causes an extracellular current flow between the two membranes. The cleft creates a resistance (R_{seal}) by which voltage is formed, directly modulating the charge dispersal across the electrode. [28].

Some simulations demonstrated that higher-frequency APs are more strongly attenuated than the lower-frequency components (such as post-synaptic potentials and membrane oscillations).

Experimental and theoretical studies revealed that R_{seal} plays a critical role in the attenuation of the FPs: the amplitude and shape of the recorded signals is inversely related to the multiplication of the value of this resistance, by the current flow across it. Usually R_{seal} is in the range of 1-2 MΩ and the consequent FPs are in the range of tens to few hundreds of μV.

The geometry and size of the sensing pad also have a wide effect on the coupling coefficient. Reducing the electrode surface area to match the neuron dimensions enhances the spatial resolution. However, this causes a greater electrode impedance and consequently a reduction of the signal-to-noise ratio (SNR). On the other hand, a larger surface could appear a good solution in order to improve the SNR: indeed this actually reduces the electrode impedance, but at the same time is more likely to gather a higher number of sources. The effect is the averaging of positive and negative

currents, which results in a reduced amplitude of the readout.

1.5 Multi-Electrode Arrays

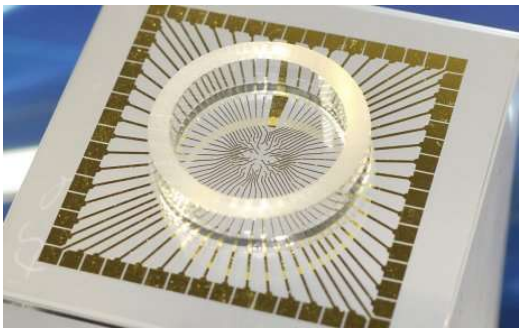

Figure 11: Example of Multi-Electrode Arrays [30].

Multi-Electrode Arrays have been broadly used to observe the extracellular electrical activity from neuron cultures. An important aim for the modern MEAs is the low impedance of the electrodes, which leads to an increase in the SNR. To achieve this goal, the effective electrode surface must be the highest possible. On the other hand, a higher electrode density improves the spatial resolution. Bio-compatibility and chemical inertness are other essential aspects to consider in the choice of the MEAs, in order to perform long-term cultures [3].

Metallic conductor electrodes – e.g., gold, platinum, titanium nitride – are widely diffused for extracellular recordings on cell cultures. A relatively high surface decreases the electrode impedance causing an SNR improvement, at the expense of the electrode density. However, using porous conductive structures – such as carbon nanotubes, graphene and doped diamond – allows a strong decrease in the electrode surface without affecting the impedance. Nowadays, the employment of active silicon-based biosensors is rapidly increasing. Field-effect transistor (FET) and complementary metal-oxide semiconductor (CMOS) technologies can be exploited to obtain high-density MEAs (HDMEAs), with the advantage of mapping a neuronal network at sub-cellular resolution. Active transducers are also becoming popular: integrating readout circuitry directly on the substrate makes possible to increase the electrode density, actively switch to multiplexing signals and improve the recording quality (low parasitic capacitance and resistance) [3].

1.6 Electrochemistry

1.6.1 Electrochemistry Basics

Electrochemistry studies the relationship between electrical energy and chemical reactions. Chemical phenomena involved in electrochemistry is associated with charge separation, which usually leads to charge transfer. This can happen in a homogeneous way in solution or in a heterogeneous way on the metal surfaces of the electrode. To guarantee electroneutrality, at least two charge transfer half-reactions occur in opposing directions [31].

A reaction is spontaneous when its Gibbs free energy (1.1) decreases. In electrochemistry a spontaneous reaction is a redox reaction and is the result of the conversion from chemical energy into electrical energy. The reverse non-spontaneous process is possible for supplying electricity. A device able to convert electrical and chemical energy (and vice versa) is called electrochemical cell.

$$\Delta G = \Delta H - T\Delta S. \tag{1.1}$$

On electrode surfaces, the charge transfer half-reactions (oxidation and reduction) are spatially separated. In an electrochemical cell this usually occurs at different electrodes immersed in the solution and connected internally and externally, via ionic transport through the solution and via electric wires, respectively. The reactions take place in the interface between the electrode and the solution.

Each electrode is associated with a potential E. The *Nernst equation* (1.2) describes the relationship between E, a standard electrode potential $E^{\ominus}$ and the electroactive species (the species involved in the redox reaction) for half-reactions at equilibrium:

$$E = E^{\ominus} - \frac{RT}{nF} \ln Q, \tag{1.2}$$

where Q (reaction quotient) is the ratio between the concentration of the reduced species and the oxidized species, R is the universal gas constant, T is the temperature in kelvins, n is the number of electrons transferred in the half-reaction and F is the Faraday constant. Thus, given the $E^{\ominus}$ values in the two half-reactions and knowing the chemical and thermodynamic conditions it is possible to predict the cell potential variations.

There are two types of electrochemical cells: electrolytic cells and galvanic cells. In electrolytic cells, when the sum of ΔG at both the electrodes is positive, the electric energy can be provided in order to force non-spontaneous redox reactions. This process is called electrolysis. The opposite happens in the galvanic cell: the total sum of ΔG at both the electrodes is negative, hence a spontaneous redox reaction generates electric energy.

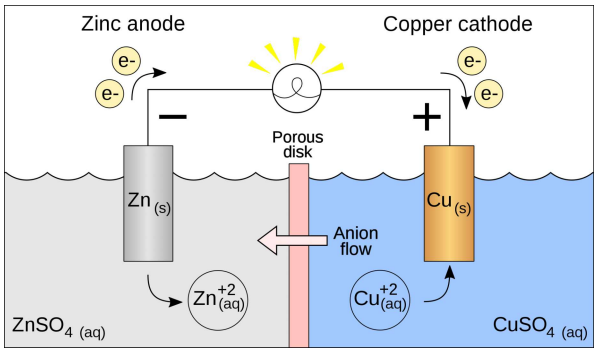

Figure 12: Representation of a basic Zn-Cu galvanic cell [32].

A basic galvanic cell is represented in **Figure 12**. In this example, the cell consists of two electrodes, one zinc (anode) and one copper (cathode), externally connected by a metallic conductor. They have been immersed in two different solutions containing the dissolved salt of the corresponding metal and separated by a porous barrier, which enables ions to diffuse through. With this configuration the zinc electrode starts oxidizing, causing the generation of Zn^{2+} ions and two electrons, free to flow through the external circuit and reach the copper electrode [33]. In the latter, the Cu^{2+} ions located in the solution around the electrode react with the two free electrodes, producing a discharged Cu atom at the copper electrode's surface. The two half-reactions are summarized below:

$$oxidation : Zn_{(s)} \rightarrow Zn^{2+} + 2e^{-} \tag{1.3}$$

$$reduction : Cu^{2+} + 2e^{-} \rightarrow Cu_{(s)} \tag{1.4}$$

This example includes metal-metal ion electrodes, but there are many other different types of electrodes commonly used in electrochemistry.

Most of the electrochemical measurement experiments focus on just one of the electrode half-reactions. However, it is always necessary to have at

least two electrodes in order to ensure the electroneutrality principle. Therefore, a *reference electrode* is commonly employed as the second half of the electrochemical cell. The reference electrode must be as stable as possible in terms of potential, plus easy to prepare and maintain. A typical electrode used as reference consists of a silver wire covered with silver chloride (insoluble in water). This electrode is well-known as the $Ag/AgCl$ electrode. The corresponding half-reactions can be represented as:

$$Ag^{+} + e^{-} \rightleftharpoons Ag_{(s)} \tag{1.5}$$

$$AgCl_{(s)} + e^{-} \rightleftharpoons Ag_{(s)} + Cl^{-}_{(aq)} \tag{1.6}$$

The $Ag/AgCl$ electrode is a good reference electrode because it's very stable, cheap and non-toxic.

1.6.2 Electrochemical Methods of Analysis

Electroanalytical methods exploit the electrochemical process to characterize various chemical substances and media. They offer several advantages compared to other techniques. Firstly, the obtaining of the results as electrical signals is essential for achieving highly accurate and fast recordings, as well as for the automation of the analysis. Moreover, high sensitivity, selectivity and the possibility to test very small volumes ($< 1mL$) are favourable features, which distinguish electrochemical methods [34] [35].

The main categories of electroanalytical methods are:

- *Potentiometry*, which measures the open-circuit potential between two electrodes.
- *Voltammetry*, which measures the current after applying a constant and/or varying potential at an electrode's surface. An important voltammetry subcategory is *amperometry*, often used in electrophysiology to study quantal release.
- *Conductometry*, which measures the electrolyte solution's conductivity.
- *Coulometry*, which measures the amount of charge consumed to fully reduce or oxidize all of the electroactive species in the solution.

In this work two groups of methods will be considered: *potentiometry* and *amperometry*.

Potentiometry

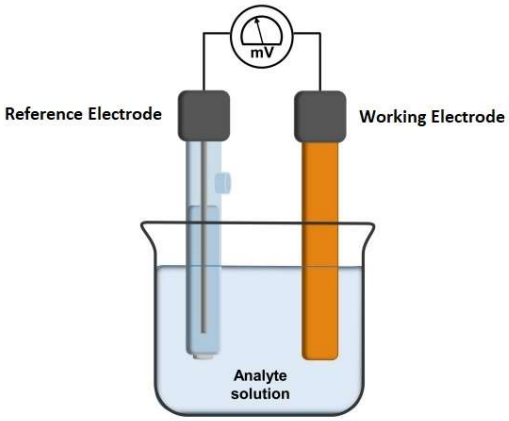

Figure 13: Simple representation of a two-electrodes potentiometric experimental set-up [36].

Potentiometry is an electroanalytical method which passively measures the potential between two electrodes under static conditions, using a high impedance voltmeter. High impedance is critical since it ensures the equilibrium of the system, reducing the current flow to negligible values. The simplest potentiometric set-up consists of two electrodes immersed in a solution: the *working electrode* (WE) and the *reference electrode* (RE). The latter's potential is known and usually is set to ground.

Potentiometry is usually employed to study the amount of analyte in a sample, exploiting the Nernst equation (1.2). Moreover, potentiometric techniques can be used in electrophysiology to detect the spontaneous electrical activity generated from excitable cells, which might cause potential variations at the working electrode [36].

Amperometry

Amperometry is a widely-used electroanalytical technique based on the measurement of currents when a constant potential is applied between two electrodes immersed in a solution, containing the analyte of interest. The constant potential is applied to the system either to reduce or oxidize the analyte at the electrode surface. This causes the generation of a current proportional to the amount of analyte, according to Faraday's law of electrolysis (1.7):

$$M = \frac{Q}{Fz} \quad [mol] \tag{1.7}$$

which links the amount of substance produced (M) with the amount of charge (Q), the valency (z) and the Faraday constant ($F = 96472\ C/mol$) [37].

To ensure the process, an optimum value of the constant potential must be applied. This needs to be set in the correct range: it must be enough to oxidize (or reduce) the analyte, but (in case of a biological application) not too high that it damages the cells [38].

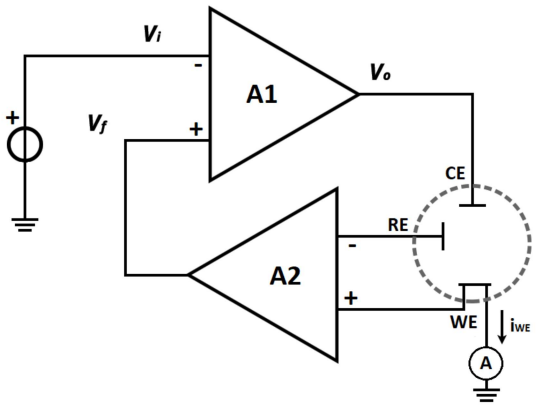

Figure 14: Example of a three-electrode potentiostat.

A common amperometric configuration is the three-electrode system, combined with a control circuit: this device is called *potentiostat*.

As shown in the example of **Figure 14**, the potentiostat has the function to apply a stable potential difference (V_i), specified by the user, between the *reference electrode* (RE) and the *working electrode* (WE) by using a negative feedback mechanism. For this purpose, a third electrode, called *counter electrode* (CE), is connected to the output (V_0) of an operational amplifier (A1). RE and WE_{sense} are both connected to the two inputs of a second amplifier (A2). The A2 output is the feedback potential (V_f) and is fed into the A1 non-inverting input, while V_i goes into the inverting one. If V_f is different from V_i, A1 starts varying V_0 until they equalise [39].

To summarise, when there is a variation in the potential difference between RE and WE, this feedback mechanism restores the set conditions by modifying the CE potential.

WE is the electrode from which the current is taken and measured.

Amperometry has proven to be one of the most suitable techniques in neuroscience when it comes to studying neurons' vesicle exocytotic release, also known as quantal release, due to advantages such as high sensitivity and optimal time resolution [40].

1.6.3 Typical Potentiometric and Amperometric Recordings

It's fundamental for the purpose of this work to understand what to expect from the potentiometric and amperometric recordings, in order to design a functional read-out device and correctly interpret the results.

Of course, a perfect prediction is impossible due to several variables that influence the readout. As seen in section 1.4, the extracellular recording with MEAs induces distortions and attenuation of the signal. Moreover the neurons may act differently based on the culture's status, for example, the number of days the suspension spent in vitro (DIV), the health condition of the cells, the nature of the medium and so on [41]. The distance between the neuron and the electrode is also important to consider: an overlap between a neuron and a sensing pad enhances the quality of the readout, whereas a higher distance causes a more attenuated and warped signal. Environmental aspects must also be considered, such as background noise and other types of interference.

In this thesis, **potentiometry** will be used to record the electrical activity of neurons. A typical potentiometric spike (**Figure 15**), generated by the AP firing from the neuron, exhibits a bipolar waveform with a steep downward deflection, followed by an upward deflection. The former corresponds to the depolarization phase of the AP's waveform and the latter matches the re-polarization phase.

It's possible to assume reasonable potentiometric spike amplitudes in the range of a few tens to a few hundreds of μV [28] [42]. *Tomagra et al.* [17] studied the recording of spontaneous firing activity of midbrain dopaminergic neurons: the mean amplitude of the peak corresponding to the depolarization phase was -50.2$\pm$3.6 μV, whereas using conventional MEAs the mean peak amplitude arrived to -54.0$\pm$4.7 μV.

Spontaneous electrical activity in neuronal networks with different archi-

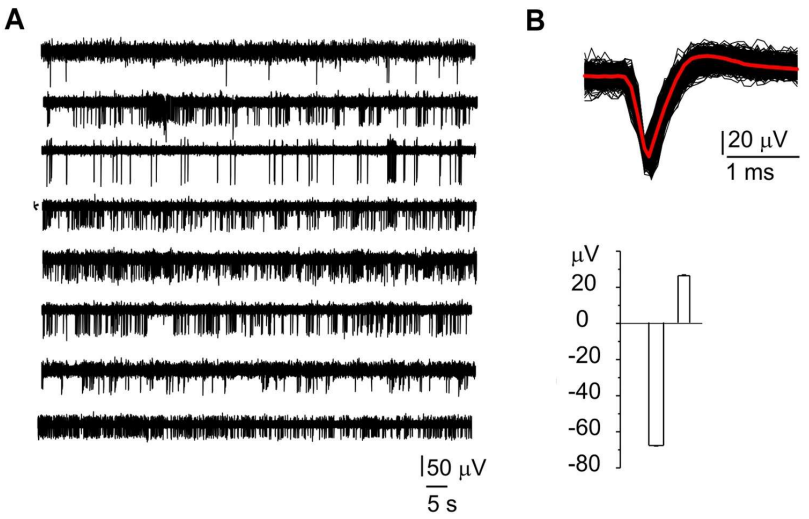

Figure 15: Potentiometric recordings from conventional MEAs. **(A)** is an example of a recorded spontaneous firing activity of cultured dopaminergic neurons from the midbrain. **(B)** Top: representation of potentiometric spikes, aligned and averaged (red trace). Bottom: bar histogram illustrates the mean amplitudes of the two peaks (negative and positive) [17].

tecture and functions shows similar behaviors in terms of firing frequency [43] [44] [45]. Many studies showed that the FPs have a firing frequency distribution with a peak at the low-frequencies (usually <1 Hz) and which becomes flat for higher-frequencies(>15-30 Hz). *Mazzoni et al.* [46] studied the dynamics of spontaneous activity in neuronal networks (rat hippocampal neurons and intact leech ganglia). For both the networks, in normal conditions, the power spectrum decreased as 1/f from 0.1 Hz to 1 Hz and became flat for frequencies higher than 2 Hz. *Tomagra et al.* [17] evaluated the distribution in frequency-domain of the potentiometric recordings of the spontaneous activity of midbrain dopaminergic neurons. The firing frequencies were comprised between 0.1 and 15 Hz, but most neurons fired with a basal frequency lower than 4 Hz and a mean firing frequency of 0.90±0.10 Hz using a conventional MEA. On the other hand, a minority of the neurons fired with a mean frequency value of 6.4±0.5 Hz (**Figure 16**).

Summarizing, the typical potentiometric spike has the following characteristics:

- Amplitude: 10 to 500 μV.
- Duration: few ms.

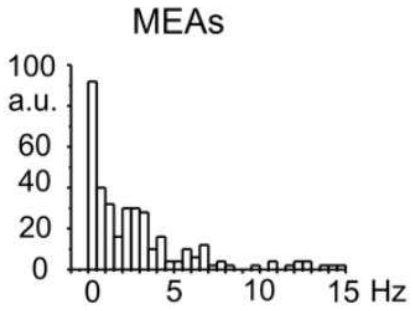

Figure 16: Firing frequency distribution for a conventional MEAs recording. Number of data are reported as percentages [17].

- Firing frequency: 0.05 to 30 Hz.

Amperometry will be applied in this work to detect in real-time the neuronal quantal release of neurotransmitter into the synaptic cleft.

The amperometric spike is characterized by a positive peak and its shape depends on the number of neurotransmitter molecules involved in the exocytosis process and on the distance from the electrode.

The amperometric trace enables not only quantitative measurements of the neurotransmitter released during exocytosis, but also kinetic information about the process [47].

The recording usually shows three different stages within the quantal release event, such as a pre-spike foot (a slow rise from the baseline representing the leakage of neurotransmitter during an early stage of vesicle fusion), a quick increment (which indicates the increase of neurotransmitter flux) and a slower exponential decrease [48]. The parameters usually taken into account to evaluate an amperometric spike are:

- The peak of the spike, which corresponds to the maximum oxidation current. Its value typically ranges from a few units to tens of pA [17] [49].
- Amplitude and duration of the foot (< 50 ms).
- Spike area, from which it's possible to estimate the number of molecules of a neurotransmitter during an exocytosis event.

Examples of amperometric recordings and typical spike shapes are illustrated in **Figure 17**.

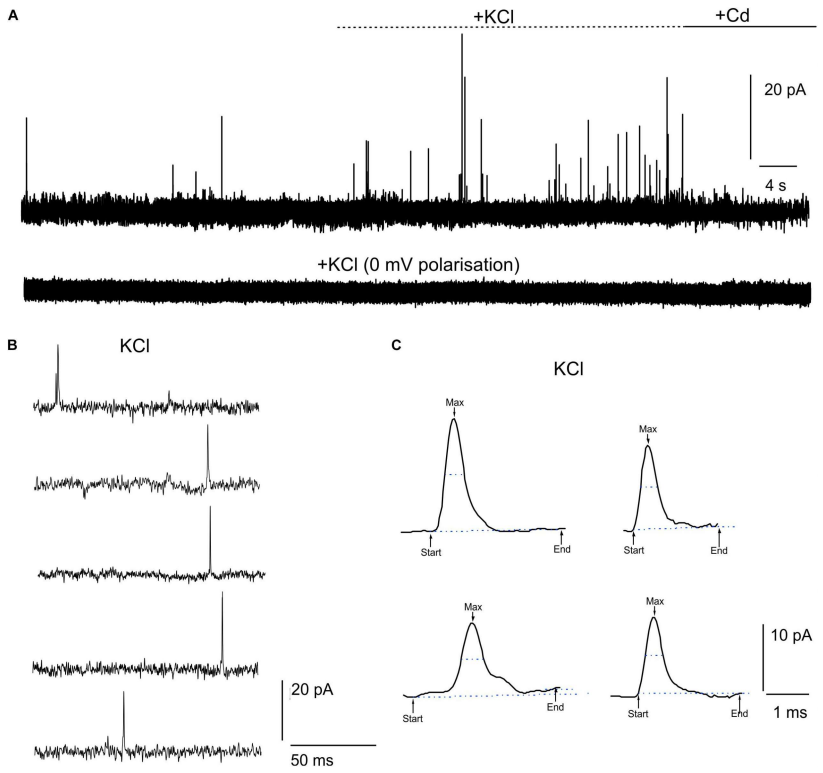

Figure 17: Amperometric recording of dopamine quantal release. **(A)** Top: single channel recording during spontaneous dopamine release in 2 mM $CaCl_2$ followed by 30 mM KCl stimulation, with a consequent alteration of the amperometric spikes; at the end 200 μM $CdCl_2$ have been added to suppress Ca^{2+}-dependent exocytosis. Bottom: recording with no polarization (0 mV) shows no detectable events. **(B)** Detection of quantal release from five different channels in the presence of KCl. **(C)** Typical amperometric spikes in the presence of KCl [17].

Amperometric spikes usually have a low mean firing frequency. *Picollo et al.* [50] discovered when studying exocytosis events from cultured chromaffin, that the mean frequency of the spontaneous release was low (abiout 0.12 Hz), whereas stimulating the culture with 30 mM KCl caused an increase to around 0.9 Hz. *Tomagra et al.* [51] analyzed the amperometric spikes due to quantal dopamine release from PC12 Cells: after an external stimulation with 30 mM KCl they detected a mean spike frequency of around 0.60$\pm$0.16 Hz; after a L-DOPA (a dopamine precursor) treatment no noticeable variation in the mean frequency (0.56$\pm$0.12 Hz) was found.

To summarise, we can predict a typical amperometric spike with the

following characteristics:

- Amplitude: 10 to 100 pA.
- Duration: tens of ms.
- Firing frequency: 0.1 to 2 Hz

1.7 External Pre-Amplification Stage

The amperometric and potentiometric signals acquired by the MEAs are very small (tens of pA and tens of μV, respectively), making the direct reading of the potentials and the currents impossible. Hence, a pre-amplification stage in an external device is necessary to provide suitable recordings for the user.

The operational amplifier (OA) has properties that make it the fundamental component to carry out this task. Many OA circuits and configurations exist, but for the purpose of this thesis only three of them will be discussed:

- Non-Inverting Operational Amplifier.
- Inverting Operational Amplifier.
- Transimpedance Amplifier.

1.7.1 Non-Inverting Operational Amplifier

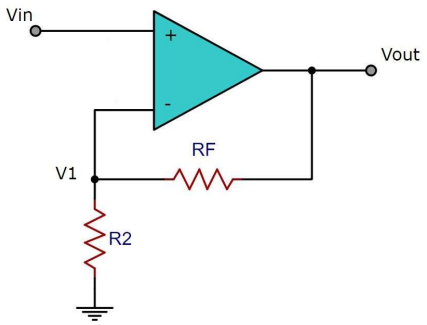

Figure 18: Non-inverting operational amplifier configuration.

A non-inverting operational amplifier (NIOA) is a circuit which amplifies a voltage signal, producing a voltage output in phase with the input. In ideal conditions, the transfer function (or closed-loop voltage gain) is:

$$A_V = \frac{V_{OUT}}{V_{IN}} = 1 + \frac{R_F}{R_2} \tag{1.8}$$

1.7.2 Inverting Operational Amplifier

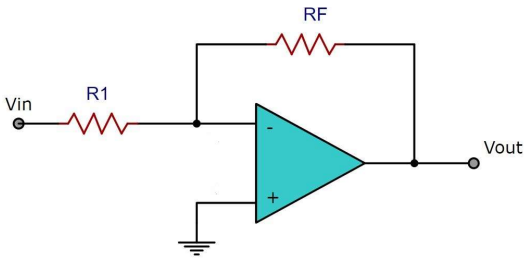

Figure 19: Inverting operational amplifier configuration.

An inverting operational amplifier (IOA) is a circuit which amplifies a voltage signal, producing a voltage output that is out of phase through 180 degrees, compared to the input. In ideal conditions, the transfer function (or closed-loop voltage gain) is:

$$A_V = \frac{V_{OUT}}{V_{IN}} = -\frac{R_F}{R_1} \tag{1.9}$$

1.7.3 Transimpedance Amplifier

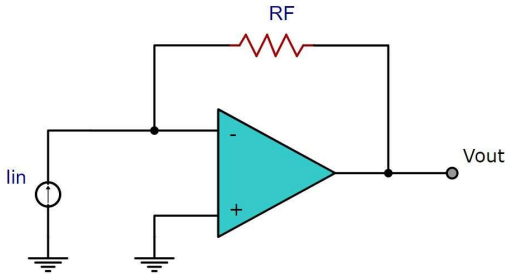

Figure 20: Transimpedance amplifier configuration.

A transimpedance amplifier (TIA) is a circuit used to convert a current input into a voltage output. The input impedance of the OA is ideally zero, hence the current can only pass through the R_F resistor. Therefore, the output voltage can be calculated as:

$$V_{OUT} = -I_{in} * R_F \tag{1.10}$$

The value of R_F can be set to determine the output voltage signal.

2 Materials and Methods

2.1 Analog Front-End

MEAs need to interface suitable electronic circuitry to readout the signal and make it available for the user. The acquisition device must respond to certain requirements which depend on the type of application. Signals emitted from cell cultures are usually at the micro-scale, thus the presence of low noise components is necessary, which amplify with a high-gain and have efficient filtering systems to reduce the interference. The pre-amplifying stages of the front-end should be placed in proximity to the electrodes to minimise the noise coupling and increasing the SNR. Depending on the application, the device may need to include a stimulation circuit. Commercially available readout platforms are suitable for a certain number of applications, but the disposal of a customized and specific system has clear advantages in terms of power consumption, dimension, compatibility with experimental conditions, adaptability and cost-effectiveness [52].

In literature it is possible to find several customized front-end electronic systems, built for specific applications. For instance, *Regalia et al.* [52] developed a low-noise low-power custom MEA interfacing system. The printed circuit board obtained has two separated stages, a preamplifier and a filter amplifier. The device has been tested and demonstrated a low input-referred noise root-mean-square (RMS) amplitude ($<\mu V_{RMS}$) and SNR similar to a commercial MEA system. Furthermore, the system has been integrated with an environmental MEA chamber to operate in the best experimental conditions.

This thesis dissertation presents an early-stage designing phase of a low-cost electronic readout circuit for interfacing MEAs for real-time monitoring of cultured neurons. The developed Analog Front-End (AFE) is a single-channel device based on multiple amplifying and filtering stages, designed to

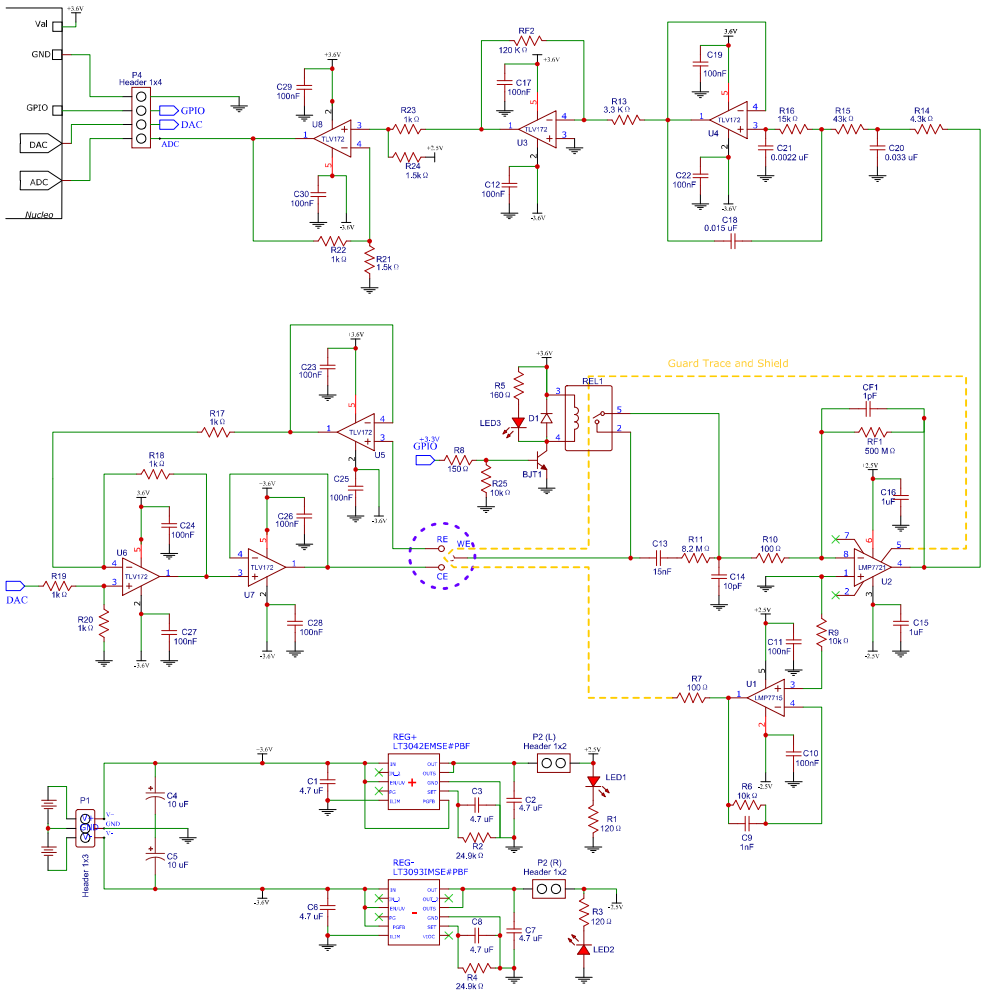

Figure 21: Complete Circuit schematic.

match the strict requirements imposed by the cell culture's electrical characteristics. Considering the low-amplitude of the field potentials collected from the cells, the noise introduced by the AFE must be small enough to enable the correct detection of the firing activity of the neurons. For this preliminary phase of the project, the goal is to obtain a signal with a maximum of 10 μV_{RMS} background noise. The complete schematic of the circuit is reported in **Figure 21**.

The device is designed to have a dual-configuration in order to perform

either potentiometric or amperometric recordings, with the possibility to select the desired modality. However, the board has mainly been tested in potentiometry which is more central for this stage of the project. The circuit for amperometry will be briefly discussed at the end of this chapter.

The AFE is based on a 55mm x 40mm four-layers Printed Circuit Board (PCB). The use of multiple layers is justified by the complexity of the circuit connections. A higher number of layers increases the attenuation of the electromagnetic interference. The top and the bottom layers are covered with solder resist, which protects the active layers from oxidation and allows it to be soldered more easily, however, in an area of the board the solder mask has been removed (this topic will be discussed in the next sections). Hence, to avoid a quick degradation of the circuit, the tracks have been covered in gold, which is resistant from oxidation.

A stitching technique has been used to ensure a strong vertical ground connection. Consequently, the ground return paths are shorter and the resistance is lower, decreasing the heat dissipation and the thermal noise.

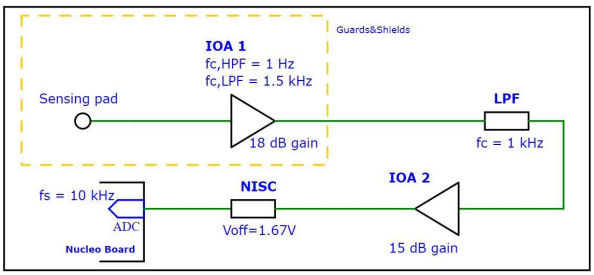

Figure 22: Simplified circuit block diagram in potentiometric mode. For the filtering stages (HPF, LPF) the cutoff frequency is reported (fc). For the amplifying stages (IOA1, IOA2) the gain is reported. For the Nucleo Board's ADC the sampling frequency is reported (fs). For the offset summer the voltage offset added to the signal is reported (V_{OFF}).

Figure 22 illustrates a simplified diagram of the main AFE's blocks. The circuit consists in the following stages:

- First inverting operational amplifier (IOA1), with a 18 dB gain. This first part of the chain is also an active band-pass filter, with a bandwidth which goes from 1 Hz to 1.5 kHz.
- Low-pass filter (LPF) with a 1 kHz cut-off frequency.

- Second inverting operational amplifier (IOA2), with a 15 dB gain.
- Non-inverting summing circuit (NISC) which sums $V_{OFF} = 1.8$ V to the output signal.
- ST Nucleo Board's analog-to-digital converter (ADC) with a sampling frequency of 10 kHz.

Figure 23 illustrates the top view and the bottom view of the AFE PCB.

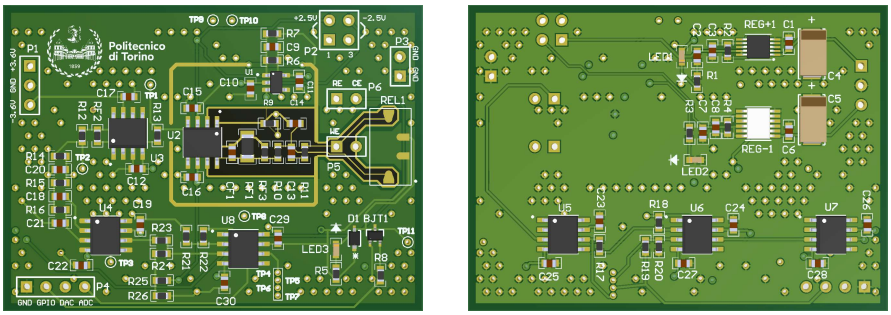

(a) Top view. **(b)** Bottom view.

Figure 23: Pictures of AFE.

Each stage is described in detail within the next sections.

2.1.1 Power Supply

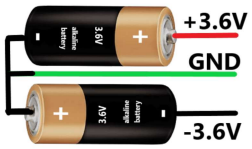

Figure 24: Two batteries connected in series, which provide a dual-voltage power supply to the board.

A pair of 3.6V alkaline batteries has been chosen to supply energy to the board. Owing to the bi-polar nature of the signal coming from neurons, both positive and negative voltages are required to feed the PCB active

components. Thus, the two batteries are connected in series to ensure the dual-voltage supply, as shown in **Figure 24**. This resulted in a ±3.6V (± V_{AL}) power supply.

In the first testing stages, the board has been tested using a bench power supply, to save battery life. For this reason, to reduce the ripple voltage generated by the circuitry, two polarized capacitors have been added between the power supply terminals.

The most critical components in the AFE's chain require a lower power supply (±2.5V), which needs to guarantee high stability and low-noise. The LT3042 positive linear voltage regulator (LVR), produced by Analog Devices is used to decrease the voltage from +3.6V to +2.5V by selecting the proper R_{SET} value (24.9 kΩ). The LT3042 is one of the best regulators in the market, in terms of performance. It is a precision ultra-low noise LVR, with a <μV_{RMS} noise. Output, input and set capacitor values have been selected, as suggested in the component's datasheet, to maintain high stability of the LVR, resulting in 4.7µF capacitance for each of them. Symmetrically, to change the negative voltage from -3.6V to -2.5V, the LT3049 negative LVR, also manufactured by Analog Devices, has been chosen. The values of the resistor and the capacitors have been chosen through the same process as the positive LVR.

Two light-emitting diodes (LEDs) have been added for giving a visual feedback to the user, to indicate if the LVRs are either correctly working or not.

The power supply circuit is placed at the bottom layer of the PCB and its complete schematic is illustrated in **Figure 25**.

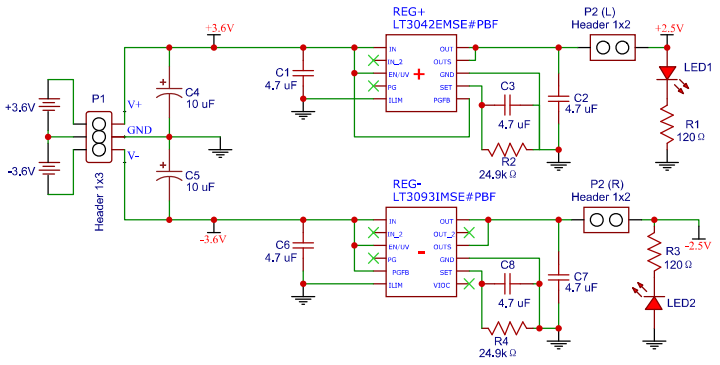

Figure 25: Power supply schematic.

2.1.2 First Amplifying and Filtering Stage (IOA1)

The first amplification stage is an IOA and it is the most critical part of the board. Aiming to have the highest SNR possible for the output signal, it is fundamental to use a precision amplifier. The LMP7721 integrated circuit by Texas Instrument (U_1) has been chosen for its optimal characteristics, including very low input voltage noise and input bias current, low consuming and high common-mode rejection ratio (CMRR). **Table 1** reports the main features of the LMP7721 precision amplifier.

LMP7721	
Features	**Values**
Input Bias Current	Max. $\pm 20fA$ at $25°C$
Offset Voltage	$\pm 26\mu V$
Offset Voltage Drift	$-1.5\mu V/°C$
DC CMRR	$100dB$
Input Voltage Noise (f=1kHz)	$6.5nV/\sqrt{\text{Hz}}$
Supply Current	$1.3mA$
Slew Rate (Falling Edge)	$12.76V/\mu s$
Gain Bandwidth (GBW)	$17MHz$

Table 1: LMP7721 Features

The LMP7721 amplifier requires a 1.8 V to 5.5 V supply voltage (supply voltage = $V_{AL}{}^{+}$ - $V_{AL}{}^{-}$). Therefore, ±3.6 V are not suitable for this component. Hence, the LMP7721 is fed by the ±2.5 V supply voltage obtained from the LVRs, which stays in the range imposed by the product constraints. To reduce the power line noise introduced by traces and other components, 1 µF decoupling capacitors were placed between the OA terminals of the power lines ($V_{AL}{}^{+}$ and $V_{AL}{}^{-}$) and the GND line, as close as possible to the integrated circuit's pads. By doing so, the noise is shunted to the GND through the capacitor [53].

The input signal needs to be amplified enough to be compatible with the resolution of the ADC. At the same time, an excessive gain can lead to the saturation of the amplifier. A neuron spike has an amplitude of the order of 10 µV to 500 µV. The ADC used in this project has a 12 bit resolution with a range of 5 V. In terms of voltage the minimum resolvable value is given by:

$$V_{MIN} = \frac{V_{RANGE}}{2^{N_b}} = \frac{5V}{2^{12}} = 1.22mV \tag{2.1}$$

The minimum gain for resolving 1µV is about 1000. For this device a 2200 global gain (33 dB) has been set, in order to reach a sub-µV resolution and correctly exploit the ADC dynamic. The first amplification stage introduces a gain of 18 dB. Knowing the gain, the relationship between the feedback (R_{F1}) and the input (R_{11}) resistors can be determined using the equation 1.9. Moreover, a constraint for R_{F1} exists, due to the amperometric configuration requiring a very high feedback resistance value (further discussed in the next paragraphs). This results in:

- $R_{F1} = 500M\Omega$
- $R_{11} = 8.2M\Omega$

The LMP7721 has a high-input resistance, which allows the use of large feedback resistors that maintain high gain accuracy despite the great loading. However, a large R_F makes the circuit particularly sensitive to its layout. Operational amplifiers always have parasitic elements affecting their performance, included the input capacitance C_{IN}. If the feedback network around an OA is resistive, C_{IN} and R_F introduce a pole, causing gain "peaking", oscillations and phase shift. Considering C_S as the total capacitance at the inverting input (including C_{IN} and further stray capacitance introduced by the traces), and R_P as the resistance obtained from the parallel between R_F and R_{IN} (**Figure 25**), the pole's frequency is:

$$f_p = \frac{1}{2\pi C_s R_P} \tag{2.2}$$

Typically, C_S in LMP7721 is 11 pF. With a low-value R_F (kΩ) the frequency of the pole is of the order of tens of MHz, high enough to have a negligible impact on stability. However, in AFE's case R_F is 500 MΩ and f_p consequently has results of the order of tens of Hz. This condition creates instability on the OA.

Inserting a feedback capacitance (C_F) in parallel to R_F can help to maintain the stability. The LMP7721 *datasheet* recommends minimum C_F values, depending on the circumstances.

If:

$$\frac{R_F}{R_{IN}} + 1 \geq 2\sqrt{GBW * R_F * C_S} \tag{2.3}$$

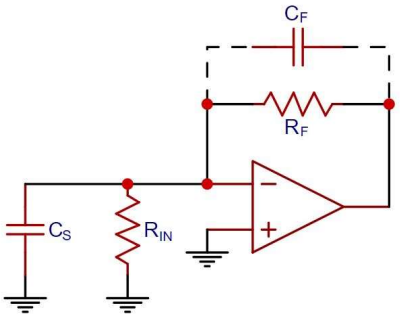

Figure 26: Example of IOA input stray capacitance.

$$\Longrightarrow C_{F,min} = \frac{C_S}{2(\frac{R_F}{R_{IN}} + 1)} \tag{2.4}$$

If:

$$\frac{R_F}{R_{IN}} + 1 < 2\sqrt{GBW * R_F * C_S} \tag{2.5}$$

$$\Longrightarrow C_{F,min} = \sqrt{\frac{C_S}{GBW * R_F}} \tag{2.6}$$

For the implemented IOA1:

$$\frac{R_F}{R_{IN}} + 1 < 2\sqrt{GBW * R_F * C_S} \tag{2.7}$$

$$\Longrightarrow C_{F,min} = \sqrt{\frac{C_S}{GBW * R_F}} = 0.036pF \tag{2.8}$$

A smaller C_F value allows an increase of the bandwidth. However, unexpected parasitic capacitance can occur. Thus, to ensure an higher stability a more conservative value of C_F should be considered. C_F in parallel with R_F creates a low pass filter with a pole frequency that is:

$$f_p = \frac{1}{2\pi C_F R_F} \tag{2.9}$$

To avoid the neuron spikes attenuation, it is necessary to chose a frequency higher than 1kHz. This creates an upper limit for the choice of the feedback value. To reach a fair compromise, the following C_F value has been picked out:

$$C_F = 0.2pA \tag{2.10}$$

$$\implies f_p \approx 1500Hz \tag{2.11}$$

A pair of electrodes in contact with the cell culture solution introduce a direct-current (DC) offset, caused by a difference in their half-cell potential due to the non-ideal similarity between them. If not considered, this offset would be amplified and could determine the saturation of the OAs. By using an offset compensation it is possible to remove the DC voltage. One way to do this is to modify the IOA1 stage to obtain an active high-pass filter and attenuate the low frequency components. Thus, a capacitor (C_H) has been placed in the inverting input line of the OA, in series with the input resistor R_{IN} (**Figure 27**).

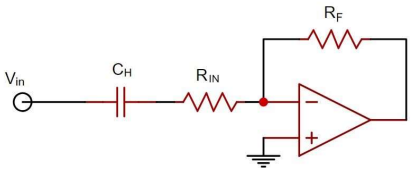

Figure 27: Active high-pass filter.

The frequency of the pole is given by:

$$f_p = \frac{1}{2\pi C_H R_{IN}} \tag{2.12}$$

To remove the DC offset it is enough to impose a f_p of about 1 Hz. For the AFE the C_H value has been selected:

$$C_H = 15nF, \tag{2.13}$$

resulting in a high-pass cut-off frequency of about:

$$f_p = 1.3Hz \tag{2.14}$$

To summarise, the IOA1 stage is both an amplifier with 18 dB gain and a first-order active band-pass filter, with a bandwidth ranging from 1.3 Hz to 1.5 kHz, approximately. At the poles, the plot's slope decreases by 20 dB/dec. **Figure 28** represents the filter amplifier magnitude and phase Bode plot.

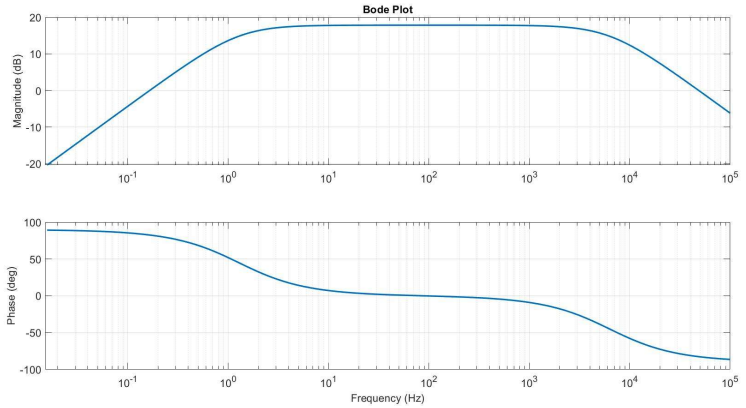

Figure 28: Bode plot of the IOA1 stage. On the top, the magnitude Bode plot is represented. Below, the phase Bode plot is represented. The two pole frequencies are $f_{p1,HPF}$=1.3Hz, $f_{p2,LPF}$=1500Hz. Both poles change the slope by -20dB/dec. The gain within the bandwidth is about 18dB.

Guards and Shields

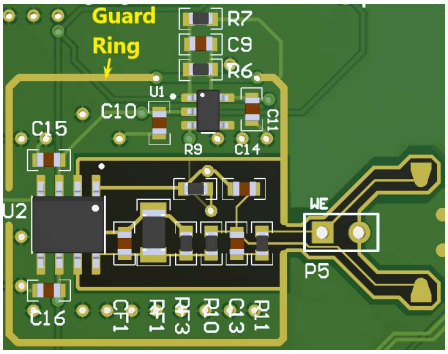

Figure 29: Picture of the first amplification and filtering stage IOA1. The golden trace which surrounds the stage is the guard ring.

When working with very small signals, parasitic leakage current and voltage perturbations coming from other components and circuitry can affect the measurement performance. For this reason a low-impedance active guard ring has been implemented to create an equal potential zone around the input pins. The ring surrounds and isolates the whole IOA1 stage and it is kept in close proximity to the input traces. For the inverting and transimpedance modes, the LMP7721 *Multi-Function Evaluation Board Users'*

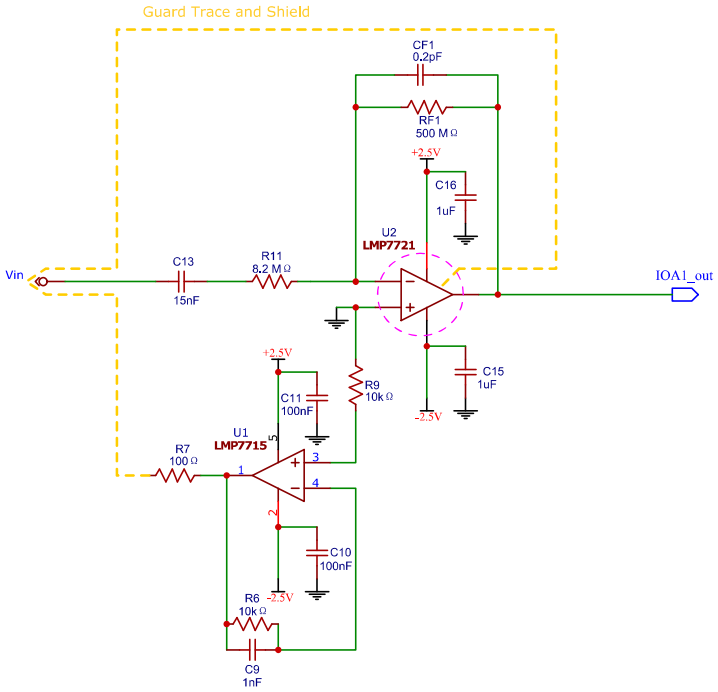

Figure 30: First amplification and filtering stage schematic.

Guide recommends driving the guard ring at the same potential as the non-inverting trace (GND). For this reason, a circuit based on the LMP7715 OA (U_1) has been inserted as an active potential driver.

R_{gd} ($= R_9$) is the resistor which connects the non-inverting input of U1 to the non-inverting input of U2. Its presence provides capacitive insulation of the non-inverting input of LMP7721. The R_{gd} value can not be too high, to avoid the creation of a pole at low-frequency bandwidths with the complicity of the input capacitance of the guard driver (about 12 pF). Therefore, 10 kΩ R_{gd} value has been selected.

R_6 and C_9 are placed in parallel as feedback elements for U1, to control the gain value (which must be kept lower than 1 in order to not cause positive feedback) and the buffer bandwidth. If R_6 has a value of 10kΩ and C_9 is 1nF, the frequency pole of the consequent low-pass filter is around 16kHz, which is suitable with the signal requirements. R_7, placed at the output of the guard driver, should be at least 100Ω to prevent disturbances caused by capacitive loading.

To guard the inputs from the power supply line, the N/C pins are connected to the guard ring, as suggested in the product *datasheet*.

Finally, the solder mask within the guard ring has been removed to reduce surface charge accumulation, which may introduce the generation of electric fields and produce unwanted effects.

Figure 30 illustrates the final and complete schematic circuit of the IOA1.

2.1.3 Low-Pass Filtering Stage (LPF)

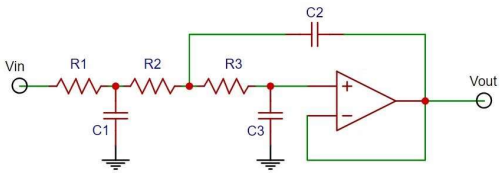

Figure 31: Third-order Sallen-Key low-pass filter.

For further attenuating the high-frequency interference, a third-order Sallen-Key low-pass filter (LPF) was included (Figure 31) [54]. This is an active filter which requires an operational amplifier: the TLV172 integrated circuit manufactured by *Texas Instrument* has been chosen. The voltage supply is dual and it is connected to the ±3.6V line. As recommended in the *datasheet*, a by-pass capacitor of 100 µF was inserted on each power supply pin to reduce errors and increase the stability.

A simplified form of the transfer function is obtained as:

$$H(s) = \frac{V_{OUT}(s)}{V_{IN}(s)} = \frac{d}{s^3 + b_2 s^2 + b_1 s + b_0} \tag{2.15}$$

Where:

- $b_2 = \frac{1}{C_1 R_1} + \frac{1}{C_1 R_2} + \frac{1}{C_2 R_3} + \frac{1}{C_2 R_2}$
- $b_1 = \frac{1}{C_2 C_3 R_2 R_3} + \frac{1}{C_1 C_2 R_2 R_3} + \frac{1}{C_1 C_2 R_1 R_3} + \frac{1}{C_1 C_2 R_1 R_2}$
- $b_0 = \frac{1}{C_1 C_2 C_3 R_1 R_2 R_3}$
- $d = \frac{1}{C_1 C_2 C_3 R_1 R_2 R_3}$

For this application, a 1.1 kHz cut-off frequency has been selected by picking out the proper resistance and capacitance values. In particular:

- $R_1 = 4.3k\Omega$, $R_2 = 43k\Omega$, $R_3 = 15k\Omega$
- $C_1 = 33nF$, $C_2 = 15nF$, $C_3 = 2.2nF$

The gain is unitary and because it is a third order filter, at the pole the slope decreases by 60dB/dec. **Figure 32** represents the filter amplifier magnitude and phase Bode plot.

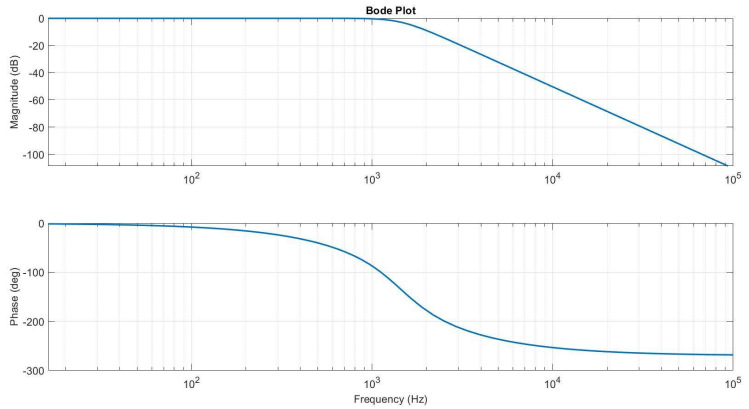

Figure 32: Bode plot of the LPF stage. On the top, the magnitude Bode plot is represented. On the bottom, the phase Bode plot is represented. The pole frequency is $f_{p,LPF}$=1.1 kHz. The pole changes the slope by -60 dB. The gain below $f_{p,LPF}$ is unitary.

2.1.4 Second Amplifying Stage (IOA2)

The IOA1 introduced a gain of 18 dB. To reach 33 dB and adapt the output signal to the ADC dynamic, a second amplifying stage (IOA2) with a 15 dB was inserted into the chain. The inverting configuration has been chosen to restore the phase of the signal, which was previously inverted by the IOA1. As in the LPF stage, the TLV172 integrated circuit has been used, with the same power supply and by-pass capacitor values.

The IOA2 is simply based on an input resistor (R_{13}) and a feedback resistor (R_{F2}). To fit the gain request, through the equation 1.9 the ratio between the resistors' values was calculated. Thus, the following pair have been selected, based on the available commercial components:

- $R_{13} = 3.3k\Omega$
- $R_{F2} = 120k\Omega$

In **Figure 33** the schematic of the IOA2 is reported.

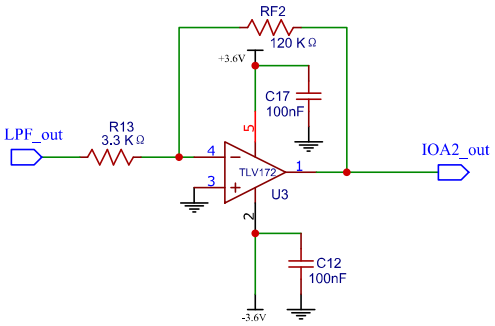

Figure 33: Inverting operational amplifier. The gain is 15dB.

2.1.5 Non-Inverting Summing Circuit (NISC)

The output signal coming from the previous stages stays within the range of ± 1.5V, considering a maximum spike amplitude of around 700 µV in absolute value. The ADC, as further discussed in the next sections, has a dynamic that goes from 0 to 5V. Hence, the ADC is not able to acquire a negative signal. To solve this problem, it is necessary to add an offset to the signal, which will be removed during the software processing. A non-inverting summing circuit (NISC) has been used for this purpose. The NISC is based on an OA: as in the previous non-critical stages, the TLV172 integrated circuit has been used, still with a power supply voltage of ±3.6V.

The offset must be high enough to translate the whole signal into positive values, but it can not exceed the power supply voltage, or it risks being saturated. Therefore, a reasonable value may be of the order of 1.5V to 2V.

The NISC is basically a non-inverting operational amplifier, with a non-inverting terminal which branches in multiple inputs: the output of the IOA2 (V_1) in series with R_1 and the +2.5V line (V_2) in series with R_2. At the inverting input terminal, the input resistor (R_i) and the feedback resistor (R_F) are present. Depending on the resistors' values, it is possible to set the offset. For this application the following resistances have been selected:

- $R_1 = 1k\Omega$
- $R_2 = 1.5k\Omega$
- $R_i = 1.5k\Omega$
- $R_F = 1k\Omega$

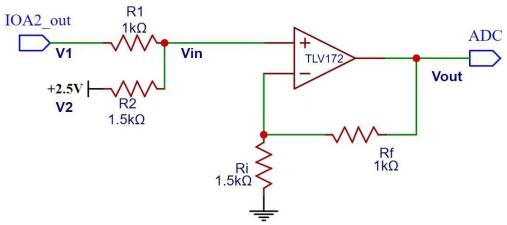

Figure 34: Non-inverting summing circuit. The resulting offset in addition to the signal is 1.67V.

Figure 34 illustrates the complete circuit schematic of the NISC.
The output voltage is:

$$V_{OUT} = V_{IN}(1 + \frac{R_F}{R_i}) = 1.67V_{IN} \tag{2.16}$$

The input voltage is given by the sum of the contributes of both the two input lines:

$$V_{IN} = V_1 \frac{R_2}{R_1 + R_2} + V_2 \frac{R_1}{R_1 + R_2} = 0.6V_1 + 0.4V_2 \tag{2.17}$$

Consequently:

$$V_{OUT} = 1.67(0.6V_1 + 0.4V_2) = V_1 + 0.67V_2 = V_1 + 1.67V \tag{2.18}$$

Therefore, with the selected resistors the offset in addition to the signal resulted in being 1.67V.

2.1.6 Amperometry

Initially, the project was set to have a dual configuration: potentiometry and amperometry. In fact, the amperometric circuit has been designed and included in the PCB, however, this part of the circuit has not been tested yet due to a shared decision to focus on the potentiometric recordings first, as these are more important for this designing stage. This section briefly explains how the amperometric mode has been implemented.

To reduce the number of components and the cost to a minimum, the potentiometric circuit has been exploited for the amperometric recordings. A push-button enables the user to switch from one configuration to the

other, by modifying part of the first filtering and amplifying stage. Once the switch is closed, the IOA swaps to a TIA. This happens by creating a short-circuit from the input to the inverting terminal of the LMP7721 (U_2), as shown in **Figure 35**.

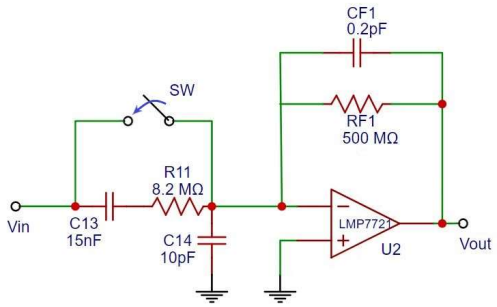

Figure 35: Switching from potentiometric to amperometric mode. By closing the switch, the configuration swaps from IOA to TIA.

In the TIA mode, the input current is amplified and converted into output voltage. By using the equation 1.10, it is possible to calculate the output voltage. The gain is given by the R_{F1} value. The TIA stage must amplify the signal to have a voltage output compatible with the subsequent stages. The typical amperometric spike has an amplitude of the order of tens of pA. Thus, with an R_{F1} value of 500MΩ (87 dB gain) the TIA stage reads out a signal smaller then 50mV.

The rest of the circuit doesn't change: the IOA2 (15dB gain) amplifies the signal to a maximum of 1.8V, while the NISC adds a 1.67V offset to fit the output with the dynamic of the ADC.

The switch to swap configuration is based on a relay controlled by an NPN bipolar junction transistor (BJT) - 2SC5876U3T106 from *ROHM Semiconductor*. The schematic of the complete relay-controller circuit is illustrated in **Figure 36**.

The selected relay (CRR03-1A produced by *MEDER electronic*) is based on a coil with a typical resistance of 70Ω. When the voltage between the two coil's terminals is high enough ($V_{DC} > 3V$), the relay acts as a closed switch. On the other hand, when the V_{DC} is small ($\approx 0V$), a negligible current flows through the coil and the relay acts as an open switch. The upper terminal of the coil is connected to the +3.6V line.

The value of current and potential through the coil is controlled by a

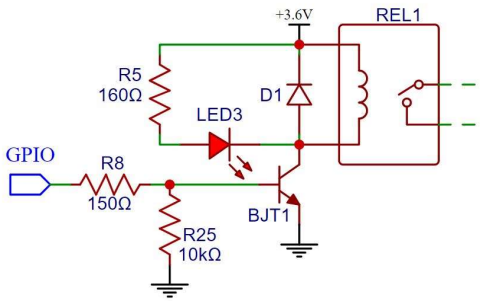

Figure 36: Schematic of relay-controller circuit.

NPN-BJT. The BJT changes the status (saturation or interdiction) depending on the base current (I_B). For this application, the base current is provided by the general purpose input/out (GPIO) port of the ST Nucleo Board. By pressing a button located on the Nucleo Board, the GPIO voltage (V_{GPIO}) can be swapped from 0 to 3.3V or vice versa.

When V_{GPIO} is 0V, no I_B flows and the BJT is interdicted. In this condition the collector current I_C (which is the same as the coil current) is negligible and the switch is open.

Inversely, if the GPIO voltage is 3.3V, I_B is not zero and it is given by:

$$I_{B,min} = \frac{V_{GPIO} - V_{BE,max}}{R_B} \tag{2.19}$$

where:

- $V_{BE,max} = 1V$
- $R_B = 150\Omega$

Therefore, I_B is at least 15mA, high enough to saturate the BJT and the current is free to flow from the collector to the emitter. The voltage between the coil's terminals resulted in:

$$V_{COIL} = +3.6V - V_{CE,sat} \tag{2.20}$$

where $V_{CE,sat} = 300mV$ (considering the maximum value reported in the product datasheet). V_{COIL} resulted in being greater then the 3V threshold required to close the switch. Under these conditions, the first stage is set in TIA configuration.

A red LED is placed in parallel to the coil to reveal the status of the relay. When the V_{COIL} is lower than the threshold the LED is off, indicating that potentiometry is the current mode. When the V_{COIL} overcomes the 3V value the LED turns on, which means that amperometry is active.

Amperometry needs a constant and stable potential to be applied to the cell culture. Hence, a three-electrode potentiostat circuit has been included in the PCB. The circuit is inspired by the work of *Aremo et al.* [55], which developed a simple and inexpensive potentiostat circuit (**Figure 37**).

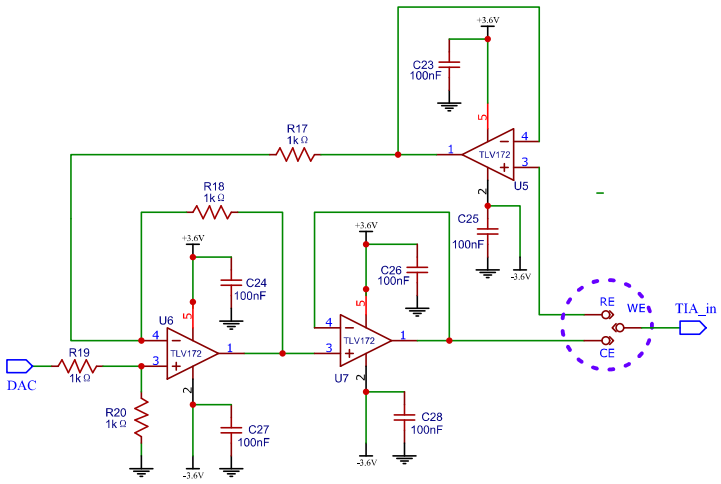

Figure 37: Complete schematic of the potentiostat circuit.

The potential value is set by using a digital-to-analog converter (DAC) of the ST Nucleo Board. A default 0.8V potential is applied, but it can be modified depending on the application.

2.2 Nucleo Board

The AFE is interfaced with an STM32 Nucleo-64 development board with STM32F446RE Micro-Controller Unit (**Figure 37**), manufactured by *STMicroelectronics*). The Nucleo board performs a certain number of necessary tasks. Primarily it is used to interface the AFE with the computer, acquiring the output processed signal from the PCB via ADC and sending the digital data to the PC via Universal Serial Bus (USB). In the amperometric mode the GPIO and DAC ports of the Nucleo board are used.

In summary, the Nucleo board is charged with the following functions:

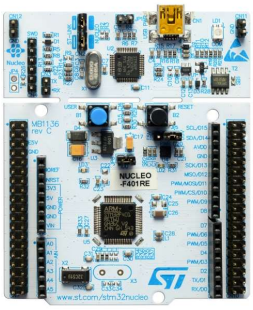

Figure 38: STM32 Nucleo-64 development board with STM32F446RE Micro-Controller Unit. The image comes from the ST website.

- ADC to acquire and convert to digital the AFE output signal with a sampling frequency (f_S) of 10 kHz.
- USB-OTG to send the converted data to the PC in real time.
- GPIO to switch the two available AFE's configurations.
- DAC to set the potentiostat potential value.

The Nucleo board's micro-controller unit (MCU) must be programmed to perform these tasks. For this purpose it integrates the ST-LINK/V2-1 debugger/programmer. After installing the necessary drivers, the ST-LINK can be connected to the operating system via USB. In doing so, it is possible to program the debugger/programmer circuit with an external application. For this application, the STM32CubeIDE software integrated development environment has been used. This software supports C, C++, Pascal and JAVA programming languages: for this project, the program was written in C-language. Moreover, the STM32CubeMX graphical tool has been utilized for generating the initialization of the C-code. Both the STM32CubeIDE and STM32CubeMX software are released by *STMicroelectronics*.

As default, the power supply of the Nucleo board is provided directly from the PC (+5V) via ST-LINK USB. However, it is possible to modify the jumper states to receive supply from the +3.6V battery. The GND of the Nucelo must be the same as the AFE's. For this reason, the Nucleo's GND connector must be connected with a wire to the AFE's GND connector.

If the PC is supplied by the power-line, the recordings are slightly noisier. Hence, it is recommended to disconnect the power cable during testing.

2.2.1 Analog-to-Digital Converter

The first step for acquiring the signal is to convert it into digital data using an ADC. The Nucleo board offers three 12-bit ADCs: ADC1 has been chosen for this application. Considering the neuron spike time-width (around 1ms), a sampling frequency (f_S) of 10 kHz has been chosen to accurately represent its shape.

In order to have the exact f_S, the ADC is triggered by a timer (TIM2). The timer clock is set by the system clock (f_{HCLK}), which is 72MHz. To reach the desired frequency, it is necessary to configure the counter settings: if the timer updates an event every time that 7200 periods are counted, the ADC conversion is triggered with a frequency of:

$$f_S = \frac{f_{HCLK}}{N_{counts}} = \frac{72MHz}{7200} = 10kHz \tag{2.21}$$

Therefore, every 0.1ms a sample is converted into digital data.

The ADC is connected between the Nucleo Board's A0 pin and a header placed on the AFE PCB.

At each acquisition, a GPIO port is toggled. In doing so, it is easy to check if the program is working or not and if the sampling frequency is equal to the one which was set.

The ADC is supplied between 0 V and 5V from the ST-LINK connected to the PC. Thus, the amplitude of the output signal coming from the AFE needs to be within this range.

2.2.2 USB-OTG

To transfer the data from the Nucleo Board's memory to the PC, the USB On-The-Go (OTG) full-speed specification has been used. The STM32F446RE MCU is set as USB-device, while the PC is the USB-host.

The USB connection used for the power supply and for transferring the program to the ST-LINK is not linked to the USB-OTG of the MCU. The pins involved in the USB-OTG communication (Data+, Data-) are located in the CN10 header of the Nucleo board. Data+ and Data- are represented by the PA12 and PA11 male connectors, respectively. The USB cable contains 4 different wires: V_{CC}, GND, USB-Data+ and USB-Data-. The cable has been modified for connecting the wires to female connectors and enabling an easy joint with the PC12, PC11 and GND connectors. The V_{CC} has been excluded, because the power supply is provided by the ST-LINK USB connector.

The device in full-speed transmits maximum 12 MBit/s, which is suitable for the f_S chosen.

Once the USB cable is connected to the PC, the operative system detects the device and a new serial port shows up as virtual COM port.

2.2.3 GPIO

To switch the AFE's configuration from potentiometry to amperometry and vice versa, the GPIO is employed, in order to drive the BJT which controls the relay-circuit. The GPIO can be set to have an output potential of either 0 V or 3.3 V. Every time a button on the board (B1) is pressed, the GPIO swaps the output.

When the button is pushed, a flag changes its value from 1 to 0. From this moment, a 500 ms delay is introduced to avoid an unwanted mechanical bouncing, which may randomly and quickly alternate the GPIO potential between 0 V and 3.3 V.

The GPIO output pin (PA10) is connected to a PCB header via wire.

2.2.4 Digital-to-Analog Converter

The DAC is necessary to apply a voltage to the potentiostat circuit input. The digital value is set within the code and is converted into an analog signal.

The DAC output pin (PA4) is connected to the AFE PCB through the correspondent connector using a wire.

2.2.5 C Program

The C program was configured by STM32CubeMX and written in STM32CubeIDE. The following code includes a small part of the program.

```
7
8  #include "main.h"
9  #include "usb_device.h"
10 #include "usbd_cdc_if.h"
11 #include "string.h"
12 #include <stdio.h>
13
14 /* Private variables */
15 ADC_HandleTypeDef hadc1;
16 DAC_HandleTypeDef hdac;
17 TIM_HandleTypeDef htim2;
18 UART_HandleTypeDef huart2;
19
```

```
/* USER CODE BEGIN PV */
uint16_t adc_val;
char msg[10]; //10 char buffer that filled up to transmit over usb-otg
float val = 0.8; //DAC output voltage value
uint32_t var; //variable to store the respective digital value
/* USER CODE END PV */

int main(void)
{
  /* Reset of all peripherals, Initializes the Flash interface and the Systick. */
  HAL_Init();
  /* Configure the system clock */
  SystemClock_Config();

  /* Initialize all configured peripherals */
  MX_GPIO_Init();
  MX_ADC1_Init();
  MX_TIM2_Init();
  MX_USART2_UART_Init();
  MX_DAC_Init();
  MX_USB_DEVICE_Init();

  /* USER CODE BEGIN 2 */
 HAL_DAC_Start(&hdac, DAC_CHANNEL_1);
 var = val * (0xfff+1)/3.3; //Conversion from voltage to the digital value
 HAL_DAC_SetValue(&hdac, DAC_CHANNEL_1, DAC_ALIGN_12B_R, var);

 HAL_ADC_Start_IT(&hadc1);

if (HAL_TIM_PWM_Start(&htim2, TIM_CHANNEL_1) != HAL_OK)
        Error_Handler();
  /* USER CODE END 2 */

  /* Infinite loop */
  while (1)
  {
    /* USER CODE BEGIN 3 */
    // Read the status of GPIO button pin
          button_val = HAL_GPIO_ReadPin(B1_GPIO_Port, B1_Pin);
    //Need to store it in the variable "button_val"
          //Check if it is high or low
          if(button_val == 0)
          {
                HAL_GPIO_TogglePin(GPIOA,GPIO_PIN_5); // If pressed toggle the LED
                HAL_GPIO_TogglePin(GPIOA,GPIO_PIN_9); // If
```

```
    pressed toggle the GPIO output
64                  HAL_Delay(500); //Delay to avoid multiple
    toggling
65                  }
66    }
67    /* USER CODE END 3 */
68  }
69
70  // ......
71
72  /* USER CODE BEGIN 4 */
73  void HAL_ADC_ConvCpltCallback (ADC_HandleTypeDef *hadc) //
    Interrupt for ADC
74  {
75          HAL_GPIO_TogglePin(GPIOA, GPIO_ADC_Pin); //At each
    acquisition, the GPIOA is toggled
76          adc_val = HAL_ADC_GetValue(&hadc1);
77          sprintf(msg,"%d\r\n",adc_val);
78          CDC_Transmit_FS((uint8_t *)msg, strlen(msg)); //Send the
     data to the PC via USB
79  }
80  /* USER CODE END 4 */
```

2.3 Post-Processing and Graphical User Interface

As soon as the Nucleo board has sent the data to the PC via USB, a software program is required to post-process the signal. A graphical user interface (GUI) has been implemented to plot the recordings in real-rime and save the results. These operations have all been performed by using MATLAB software. The main code sections are reported in this paragraph.

Firstly, constants are defined as follows:

```
7  % Constants
8  fs=10000; %Sampling frequency
9  fNy=fs/2; %Nyquist frequency
10 Ap=500*120/(8.2*3.3); %Total amplification in case of
    POTENTIOMETRIC config.
11 Aa=500*10^6*120/3.3; %Total amplification in case of
    AMPEROMETRIC config.
```

In order to perform the two configurations (potentiometry and amperometry), a question dialog is involved to enable the user to select the desired

modality. Depending on the selected answer, certain parameters are set, to adapt the graph to the type of recording.

```
% Question Dialog
answer = questdlg('Select the configuration', ...
        'Read Out Device Configuration', ...
        'Potentiometry','Amperometry','Escape','Escape');
% Handle response
switch answer
    case 'Potentiometry'
        disp([answer])
        A=Ap;
        E=10^6;
        tit=answer;
        yName='Measured Voltage (uV)';
        lim1=-100;
        lim2=100;

    case 'Amperometry'
        disp([answer])
        A=Aa;
        E=10^12;
        tit=answer;
        yName='Measured Current (pA)';
        lim1=-100;
        lim2=100;
    case 'Escape'
        return
end
```

The next step concerns the connection of the serial port, specified by the virtual COM port, to enable communication between the serial object and the algorithm.

Before connecting the port, the *instrreset* command is used to delete all open instrument objects, in order to avoid conflicts with the virtual COM port. The serial port is then identified and opened. The properties are set as default.

```
% Serial Object
%Disconnect and delete all instrument objects
instrreset
% Connect the serial port
s = serial('com6');
fopen(s)
```

Once the port is open, a while-loop is used to create the graph. At the beginning of each cycle, the data array is filled with 100 samples to reduce the plot's updating frequency and consequently, the computational effort.

The data is converted into the correspondent AFE's output voltage value. Then, the offset value introduced by the NISC (+1.67V) is subtracted and the amplification removed, to complete the estimation of the original input signal.

The plot has been designed to have a sliding time-window, for an user-friendly real-time representation of the recording.

A break-button is placed on the graph edge, in order to interrupt the recording and proceed with the whole-signal analysis.

```
% Main Loop
i=0; %Definition of indexes
j=0;
t1=0;

% Break Command
DlgH = figure;
H = uicontrol('Style', 'PushButton', ...
                    'String', 'Break', ...
                    'Callback', 'delete(gcbf)');

while (ishandle(H))
    for j=1:100 %Collect 100 samples
        i=i+1;
       data(i)=str2double(fscanf(s));
    end
        if i<=5000 %First 5000 samples
            x1=rmmissing(data); %Remove missing entries
            % Digital number -> Voltage (or current)
            y1=x1*3.3/4096;
            y1=(y1-1.667)/A*E;
            % Time-scale
            t1=1/fs:1/fs:length(y1)/fs;
        else   %After the first 5000 samples
            x1=rmmissing(data); %Remove missing entries
            % Digital number -> Voltage (or current)
            y1=x1(end-4999:end)*3.3/4096;
            y1=(y1-mean(y1))/A*E;
            % Time-scale
            t1=(length(x1)-length(y1)+1)/fs:1/fs:length(x1)/fs;
        end
        plot(t1,y1);
        xlim([t1(1) t1(end)+2]);
        ylim([lim1 lim2]);
        grid on
```

```
93          title(tit)
94          xlabel('time (s)')
95          ylabel(yName)
96          drawnow
97  end
98  fclose(s);
```

After the interruption of the real-time streaming, a dialog box interacts with the user. If desired, it is possible to proceed with the processing and representation of the whole recorded signal.

```
91  % Whole Signal Representation
92
93  %Dialog Box
94  answer = questdlg('Would you like to see the whole signal?', ...
95    'Whole signal representation', ...
96    'Yes','No','No');
97  % Handle response
98  switch answer
99      case 'Yes'
100         disp('Whole Signal Representation')
101     case 'No'
102         clc
103         return
104 end
```

The data is then processed for removing the 50 Hz power-line interface. For this purpose, an infinite impulse response (IIR) digital notch filter with 50 Hz rejection has been implemented (**Figure 39**) and applied.

The whole processed signal is plotted and saved.

Finally, for analysis of the recording in the frequency domain, the power spectral density is employed using the Welch's method. The results are displayed on a graph.

```
157 %% Power Spectral Density
158
159 NFFT = fs/0.125;
160 [Pxx1,f1]=pwelch(y2,rectwin(600),0,NFFT,fs);
161
162 figure()
163 plot(f1,(Pxx1)/max(Pxx1),'LineWidth',2);
164 xlabel('Frequency (Hz)','FontSize',20)
165 ylabel('Power Spectral Density','FontSize',20)
166 axis([0 2000 0 1])
```

```
167 set(gca,'FontSize',20)
```

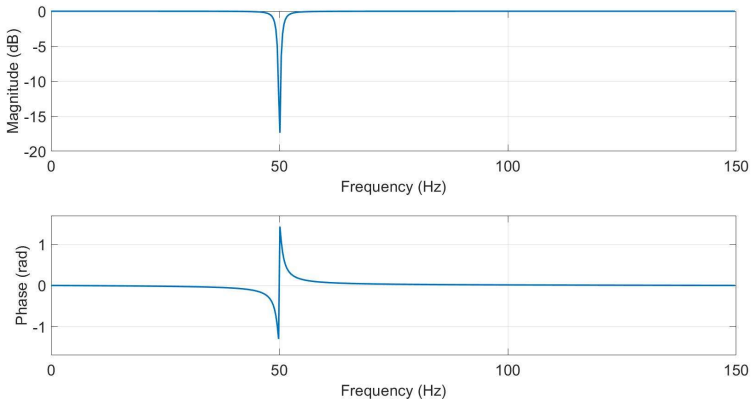

Figure 39: Frequency response of a digital notch filter with 50 Hz rejection for power-line interference attenuation. Above, the magnitude frequency response is represented. Below, the phase frequency response is represented.

2.4 Multi-Electrode Arrays

Diamond-based MEAs (D-MEAs) have gathered interest in the last years. Thanks to the meta-stable nature of this allotropic form of carbon, diamond can be turned into graphene, which is conductive. By varying the doping level of specific regions, micro-graphitic electrodes embedded in the diamond substrate can be created. One of the most widely used techniques to induce this phenomenon is ion implantation, followed by heat treatments.

Picollo et al. [56] developed a 16-channel D-MEAs for cell cultures. Ion implantation and annealing processes were employed to create highly-damaged regions in the diamond's structure and convert them into a graphitic phase. A 1.2 MeV focused beam of helium ions (He+) was shot on single-crystal diamond micrometric sub-superficial structures to cause the damage. Then, by the annealing of the sample, the conversion was completed. Micro-graphitic electrodes, embedded into the diamond substrate, were then created.

The implantation was performed at the AN2000 accelerator of Legnaro (Italy).

The micro-graphitic electrodes are connected to 2 arrays of 8 pads, located outside of the perfusion chamber.

Figure 40 shows the 16-channel D-MEAs with a zoomed image of the micrometric graphitic electrodes at the centre of the perfusion chamber.

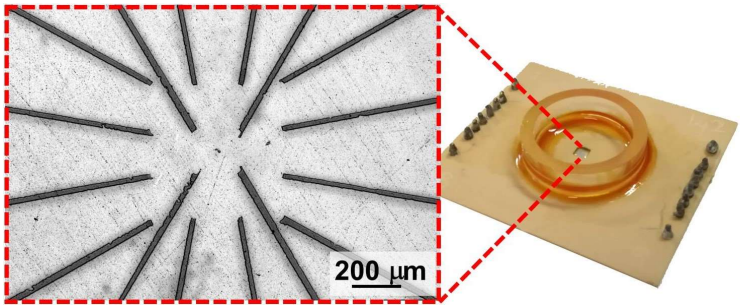

Figure 40: On the right are the 16-channel MEAs based on micrometric graphitic electrodes embedded into a diamond substrate. On the left, a microscopic image of the graphitic electrodes. [17]

D-MEAs present favourable characteristics in comparison to conventional MEAs, in terms of insulation properties, bio-compatibility, transparency, thermal conductivity and mechanical robustness [57].

To evaluate the biosensor's performance, cyclic voltammetry and amperometry measurements have been undertaken on solutions by progressively increasing the concentration of adrenaline. Studies conducted by *Tomagra et al.* [17] [51] proved the quality of D-MEAs with amperometric and potentiometric recordings on primary cultures of mesencephalic dopamine neurons from substantia nigra (SN).

The aim of this project is to produce an electronic system for interfacing these types of MEAs. However, the AFE board has not been tested directly on the 16-channel D-MEAs, for a few reasons. To evaluate the performance it was necessary to compare the results with a commercial system. The USB-MEA60-Inv-BC-System provided by the University of Turin was the only available device for performing potentiometric recordings. This is configured for interfacing 60-channels MEAs, hence it is not suitable for the current 16-channels D-MEAs. Moreover, working with 60-channel MEAs as opposed to 16 is far more rewarding from a scientific point of view.

As seen above, the D-MEA quality has already been evaluated through several experiments, conducted by *Tomagra and colleagues* and other research groups. Thus, for this early-stage designing phase of the AFE, the

goal is to demonstrate that it works and that the performance is comparable to the USB-MEA60-Inv-BC-System. Therefore, for the first testing stages, the AFE board has been interfaced to commercial MEAs. If the expected results are confirmed from the experiments, it is reasonable to assume that it should also work with the D-MEAs.

In the future, a 60-channel D-MEA chip will be object of study from the Department of Physics at the University of Turin, in parallel with further improvements and developments of the AFE board.

The 60MEA200/30iR-Ti from the 60StandardMEA series, manufactured by *Multichannel Systems*, is the commercial MEA used for testing the AFE. It is based on titanium nitride (TiN) electrodes embedded in Silicon nitride (SiN) insulator. Overall, there are 59 recording electrodes with a 30 µm diameter and a 200 µm inter-electrode distance and a wider internal reference electrode. The electrodes are connected to the correspondent TiN pads, from which the signal can be collected. The basement and the perfusion chamber ring are both made of glass.

2.5 MEA Adapter

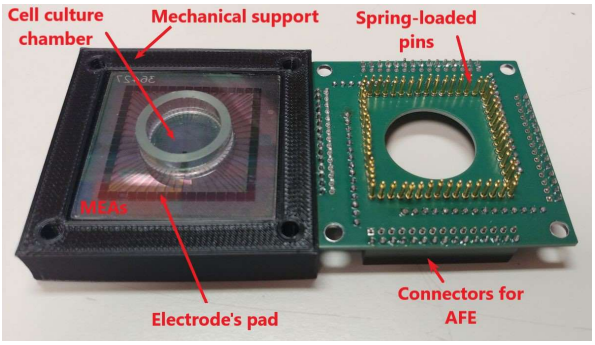

Figure 41: Adapter for MEAs. On the left, the basement where the MEAs stand. On the right, the spring-loaded pin adapter for interfacing the AFE to the MEAs.

With the purpose of interfacing the AFE to the cell culture (and consequently to the MEAs), a basement and an adapter have been designed and produced.

The basement is required to provide mechanical support to the MEAs. The component is 70mm-wide, 70mm-long and 13.4mm-high. At the vertexes, four through holes with a 4.5mm diameter are created to mechanically

couple the adaptor to the basement, via the use of M4 screws with a length of 20mm. On the bottom of the basement a hexagonal cut was made coaxially for each hole, to insert M4 hex nuts. On the top, a 51mm x 51mm square has been cut (with a depth of 1mm) for hosting the MEAs. This size has been decided considering the MEA base dimensions (49mm x 49mm x 1mm).

The basement is made with polylactic acid (PLA). It has been designed using the software SolidWorks and built with a 3D-printer.

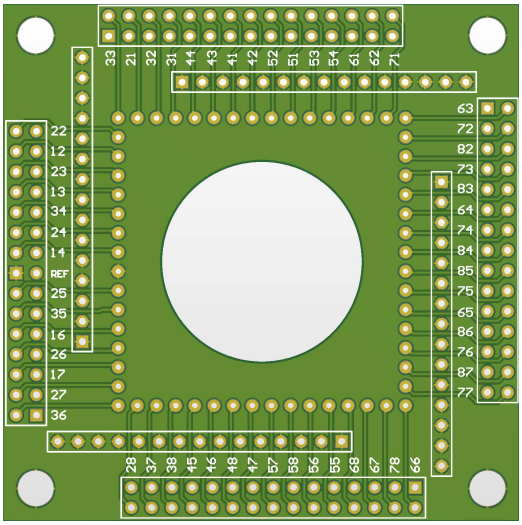

Figure 42: Adapter PCB TOP view.

The adapter is a 2-layer PCB, which aims to intercept the signal coming from the MEAs and transmit it to the AFE board. Having stable contact with the MEA pads is essential to correctly transfer the recording to the AFE. Thus, 60 spring-loaded headers (one for each MEA pad) have been soldered to the PCB. Four 4mm-diameter holes were created at the PCB vertexes, as was done on the basement. By tightening the M4 screws, the adapter is mounted to the basement. The spring-loaded headers are compressed against the MEA pads, due to the vertical force generated by the screws.

Each pin of the adapter is connected via trace to a correspondent female-header, resulting in 4 arrays of 15 connectors (**Figure 42**). Each connector has been numbered following the indications of the MEAs *datasheet*. The reference electrode, instead, is connected to the GND line by pouring copper

on one PCB layer. 60 female GND connectors (also organised in 4 arrays) are then soldered to the PCB.

To summarise, each channel corresponds to a female connector.

The channel and the GND connectors have a fixed distance between them, which is equivalent to the distance between the input (WE) and GND male-headers of the AFE board. In this way, the AFE can be easily assembled and fitted to the desired channel of the adapter without using wires and minimizing the noise introduced by connections.

An image of the assembled system is reported in **Figure 43**.

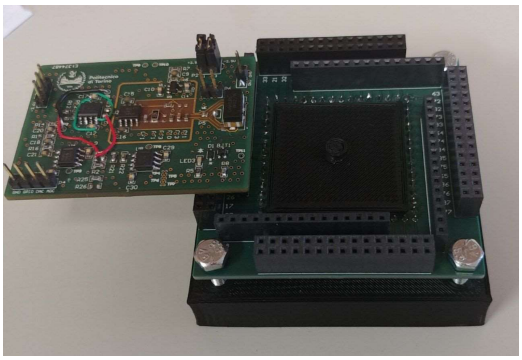

Figure 43: Picture of the AFE board assembled with the MEA'a adapter.

2.6 Cell Culture

Pruszak et al. [58], in 2009, published a protocol for preparing primary cultures of mesencephalic (or mid-brain) dopamine neurons. The same method has been adopted by the researchers of the Department of Drug and Science Technology [17].

The ventral midbrain area was dissected from the embryos of mice to grow substantia nigra dopaminergic neurons. The procedures have been performed following the European Community's Council Directive 2010/63/UE.

For the adhesion of the cells on the substrate, MEAs were coated with 0.1 mg/ml poly-L-Lysine. The neurons have been plated with a final density of 2000 cells/m^2 for each tested MEA.

After the plating, the cell cultures have been stored in an incubator with controlled temperature (37°) and CO_2 in atmosphere (5%). For the maintenance and the maturation of the neurons, Neurobasal Medium containing 1% penicillin-streptomycin, 1% ultra-glutamine, 2% B-27 supplement and

2.5% Fetal bovine serum (FBS) was used. The pH of the solutions was 7.4. The cells have grown in these conditions for 14 DIV before testing.

2.7 Tests

The AFE has been tested to verify the performance of the device and conduct experiments for scientific research. The tests have been performed under varied conditions and different locations, by configuring the board in potentiometric mode.

The most important trial to conduct was the testing of the AFE on substantia nigra dopaminergic neurons. However, one of the main problems with experimenting directly on neurons relates to the unreliability and low number of cell cultures that are available. The MEAs were plated individually and it was not always possible to guarantee the survival of the cells during the 14 DIV maturation period.

Therefore, it was necessary to find an alternative, reliable way to evaluate the board before testing it on cultured neurons. The laboratories of the Electronics and Telecommunication Department (DET) of Politecnico di Torino solved this by generating signals with similar characteristics to the potentiometric neuron's spikes. By simulating the physiological behavior of the neurons, it was possible to assess the board and adopt adjustments and improvements.

Finally, multiple sessions of tests on real cell cultures have been conducted at the laboratories of the Department of Drug and Science Technology.

The results obtained from these tests using the AFE have been compared with the recordings performed by a commercial acquisition system. The USB-MEA60-Inv-BC-System (from *Multichannel Systems*) is a commercial setup used for extracellular recordings from neuron cell cultures placed directly on the 60MEA200/30iR-Ti. Raw data from the MEAs is pre-amplified and filtered by MEA1060 filter amplifiers with custom bandwidth and gain. Then, the data is sent via USB 2.0 High-Speed to a computer.

The project aroused interest from researchers of the Molecular Biotechnology Center of the University of Turin. This led to tests being performed at their laboratories under completely different conditions.

All tests are described in detail in the next sections.

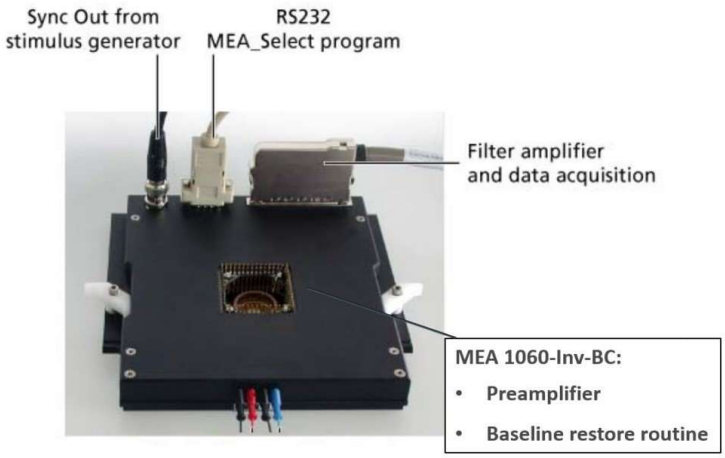

Figure 44: Picture of USB-MEA60-Inv-BC-System, taken from the datasheet available on the Multichannel Systems website.

2.7.1 Tests Under Simulated Conditions

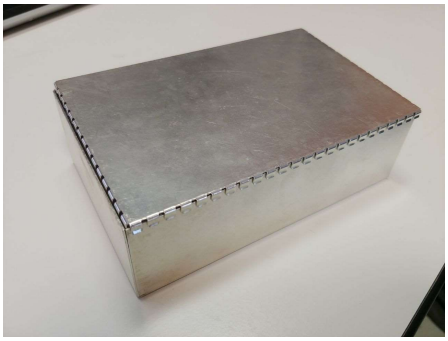

Figure 45: Cage of Faraday used for rejecting external interference.

To correctly evaluate the AFE performance, it was fundamental to reproduce similar conditions to the laboratories of the Department of Drug and Science Technology. Thus, both the neuron spike shape and the environmental electrical state needed to be similar.

The incubator where the measurements on the cell culture were conducted, works as a Faraday cage. Its ability to shield the internal environment from external electromagnetic interference and reduce background noise, results in more accurate measurements.

A Faraday cage available at the laboratories of DET was employed for

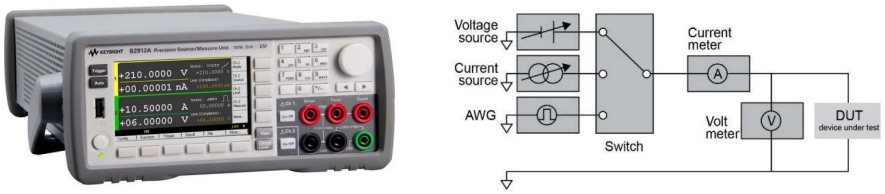

(a) Picture of the Agilent SMU.

(b) Agilent SMU configurations.

Figure 46: Agilent (Keysight) B2912A bench-top Precision Source/Measure Unit. Both images have been taken from the Keysight B2900A Series Precision Source/Measure Unit *datasheet*.

the simulation(**Figure 45**). During all acquisitions, the AFE board's GND was connected to the metallic cage.

To generate the pseudo-neuronal spike, the Agilent (Keysight) B2912A bench-top Precision Source/Measure Unit (SMU) has been selected due to the presence of its very low voltage and current sourcing capabilities. It is also possible to trigger pulses in a single mode or in sweeping mode, with variable amplitude and time-width (**Figure 46**).

The neuronal field potentials have an amplitude of tens of µV. A reasonable time-width is around the unity of the millisecond. It is not possible to reproduce a perfect neuronal spike shape, which is different every time the neuron fires. For these tests, a simple square-wave pulse was generated with similar characteristics to the desired shape. The amplitude value depended on the type of test, varying from 200 to 20 µV. The time-width was kept at 1 ms for all experiments, which is an average value for the real spike.

One of the two channels of the Agilent B2912A SMU has been connected to the input connectors of the AFE (high-force to WE and low-force to GND).

The complete set-up for the tests under simulated conditions is shown in **Figure 48**.

Under these circumstances, multiple tests have been performed. The principal of those are reported as follows:

- 0 V input without triggering the generation of the pulses, to evaluate the analysis of the noise level. The AFE's inputs (WE and GND) were immersed in plain water, to reproduce the cell culture's solution.

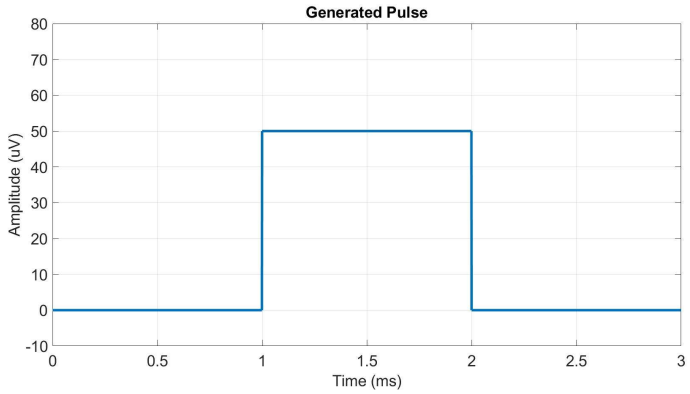

Figure 47: Square-wave pulse used for simulating a neuronal spike. The time width was set to 1ms, the amplitude varied depending on the type of test: in this case 50 µV was chosen.

- Recording with and without using the digital notch filter, with arbitrary amplitude pulse generation.
- Pulses detection, with a square-wave amplitude of 50 µV and 20 µV and 1 ms time-width.
- Introduction of a 100 mV offset to evaluate the active high-pass-filter DC rejection and the transient introduced by it.

2.7.2 Tests on Cell Culture

Experiments on real cultured neurons took place at the neuroscience laboratory of the Science and Drug Technology Department.

An inverted microscope was available for observing the neurons plated on the MEA.

All tests have been conducted within an incubator. The incubator is designed specifically for these types of applications and is able to maintain stable variables, such as temperature (29°C), CO_2 concentration (5%) and humidity (in a range of 95% to 98%). The internal part is non-corrosive and stainless, to protect the culture from contamination. The incubator is also a Faraday cage, able to reject external sources of interference.

The USB-MEA60-Inv-BC-System stood on an inner shelf. Via USB, it was connected externally to a computer placed outside the incubator. This was necessary to stream in real-time the recordings from all 60 channels of

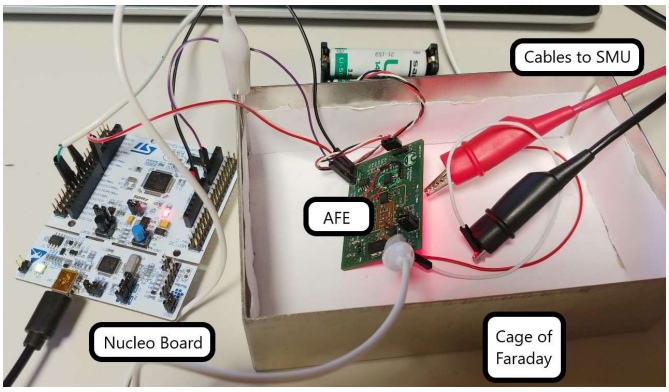

Figure 48: Set-up for tests under simulating conditions. During the tests the Faraday cage's lid is closed.

the commercial acquisition system.

After 14 DIV, the cell culture was tested using the USB-MEA60-Inv-BC-System to understand if the neuronal firing activity was present, or not. The majority of the time the neurons were inactive and the process of plating and maturation on the MEA needed to be restarted.

When the cell culture was found active, a recording of all 60 channels was performed by the commercial device to compare the results with the AFE at the end of the session.

Unfortunately, it was not possible to execute parallel and simultaneous acquisitions. During the first testing sessions, the attempts to connect the two systems to the MEA at the same time failed. This was caused by an incompatibility between the two devices, which also occurred when the USB-MEA60-Inv-BC-System was turned off.

At that point, it became necessary to isolate the MEA from the commercial circuitry. The solution was found by building the adapter, described in section 2.5.

The external power supply of the USB-MEA60-Inv-BC-System was switched off at the end of its recording, to avoid further noise affecting the AFE's results.

Then, the AFE has been assembled. First, the MEA with the cultured neurons has been located on its seat, on the mechanical support. The adapter's spring-loaded pins were pressed against the MEA's pads by tightening the screws. The AFE board's WE and GND pins were then individually fitted to each of the 60 channels. The selection of channels used

for taking measurements was decided based on the activity of the neurons detected on the USB-MEA60-Inv-BC-System recordings.

The system has been placed inside the incubator on a glass tray, to avoid creating unwanted contact with the metallic shelf. Subsequently, the device's GND line has been connected to the shelf, to maintain the same voltage as the Faraday cage. The Nucleo Board was then connected via USB with the PC with the customized GUI to transfer the data.

2.7.3 Tests on Cell Culture - Interdigitated Electrodes

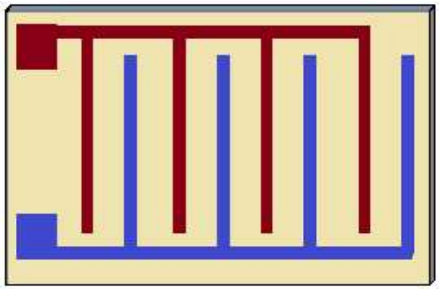

Figure 49: Simple representation of interdigitated electrodes.

At the Molecular Biotechnology Center of the University of Turin, the AFE has been tested under different conditions to those described so far. By combining two different projects, the AFE was used for taking potentiometric recordings from cell cultures, based on interdigitated electrodes. These types of electrodes are normally employed for performing measurements of impedance.

The interdigitated electrodes (**Figure 49**) have a much greater surface area when compared to the microelectrodes usually used for potentiometric recordings. Thus, the presence of a large number of neurons on an electrode causes the summation and the time filtering of signals. The consequent attenuation leads it to be impossible to detect single neuronal spikes under these conditions. However, this experiment was designed to evaluate the overall neuronal network's electrical response to the introduction into the solution of a large quantity of glutamate, a neurotransmitter which binds to receptors of the types of neurons tested.

For these recordings, the ADC was configured to acquire data with a sampling frequency of 1KHz.

A cell culture constituted by 6x8 wells and with 50.000 cells/well was used to conduct the experiment. The culture was based on primary cortical mouse neurons grown on interdigitated electrodes and maturated for 14 DIV before performing the test.

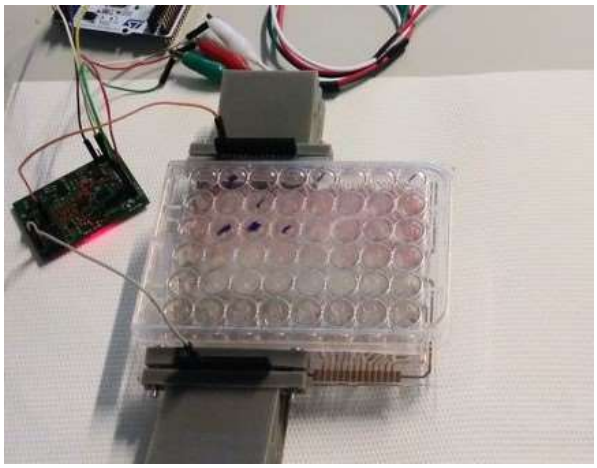

Figure 50: Experimental set-up for performing tests with the AFE interfaced with cell cultures based on interdigitated electrodes.

12 of the 48 wells have been utilized for the experiments. Two types of tests have been performed:

- Massed treatment: 6 wells have been treated once with 200 µM glutamate injected into the solution.
- Spaced treatment: 6 wells have been treated with 5 pulses of 40 µM glutamate every 20 seconds.

For these tests the Faraday cage was not used, due to the absence of a cage with suitable dimensions for containing the whole cell culture.

The system has then been assembled. The complete experimental set-up is displayed in **Figure 50**.

3 Results

The results obtained are shown in this section. First, the outcomes from the recordings in simulated conditions are reported to show the performance of the AFE. Then, tests on cell cultures are displayed to assess the quality

and reliability of the AFE's recordings, in comparison to the commercial acquisition MEA system and obtain a statistical analysis of the neuronal behavior.

3.1 Simulated Spike Recordings

The first aspect to evaluate was the background noise level. The analysis needed to be done under a state of inactivity, to reproduce as precisely as possible the experimental conditions of cell cultures. The two inputs of the device have been prolonged using two jump wires immersed in plain water, which has similar properties to the physiologic solution of the culture. The water container was safely placed inside the Faraday cage, in addition to the board, for external interference shielding.

The system has then been assembled and the recording performed. **Figure 51** shows 10 seconds of the resulting signal.

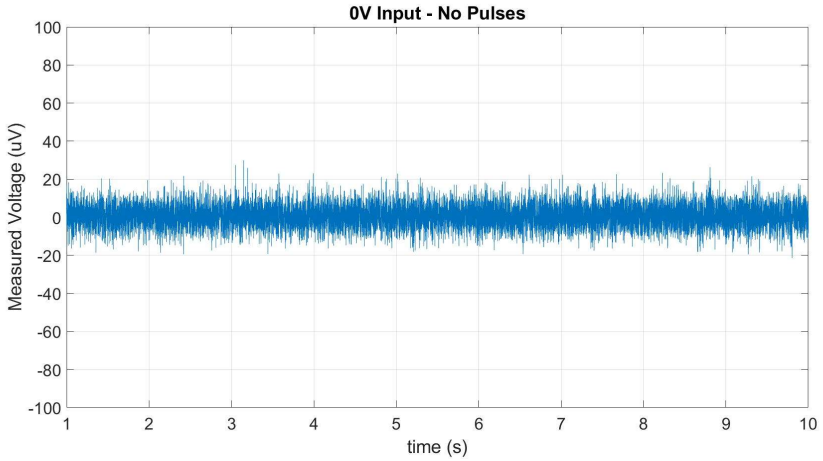

Figure 51: 10 second plot. Recording under simulated conditions, in the presence of no-activity and no-pulses generated.

The noise was first evaluated by looking at the track: the peak-to-peak signal is contained between ±20 µV. It was also calculated using the discrete RMS amplitude of the whole signal:

$$V_{n,RMS} = \sqrt{\frac{1}{N}\sum_{i=1}^{N}|V_i|^2} \tag{3.1}$$

Where:

- N is the number of samples considered.
- V_i is the voltage value of the i-th sample.

The RMS noise of the recording with no-input was has been obtained from MatLab and resulted in being:

$$V_{n,RMS} = 5.1\mu V \tag{3.2}$$

This value is lower then the threshold of 10 µV fixed at the beginning of the project. These results demonstrate that under these conditions the AFE board performed satisfactorily.

The power spectral density of the signal was estimated using Welch's method (**Figure 51**).

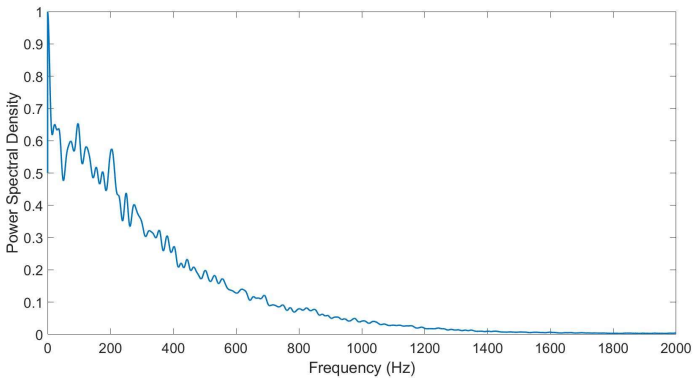

Figure 52: Power spectral density of the recording performed in simulated conditions, with 0V input and no pulses generated. The power spectral density was normalized by dividing it for its maximum value.

The effect of the digital notch filter has been evaluated. For this test, 500 µV positive pulses with no-offset were generated and sent to the AFE input. The AFE was kept outside of the Faraday cage. First, the data was acquired. The signal has then been filtered with a 50 Hz rejection notch filter and compared to the raw track. The results are shown in **Figure 53**.

The effect of the active high-pass filter, located at the input of the AFE circuit, was evaluated. To prove the DC rejection, a 100 mV offset was generated by the SMU and applied to the input of the AFE. Pulse trains of

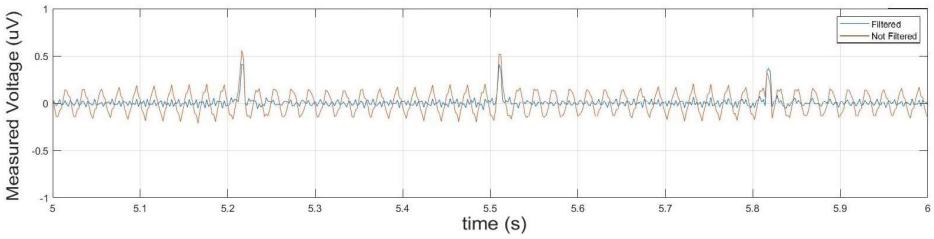

Figure 53: Not filtered track (red) VS filtered track (blue) with 50 Hz rejection notch filter.

100 µV were also sent to the input. **Figure 54** reports the results obtained. The transient introduced by the high-pass-filter proves that the DC offset has been exponentially removed.

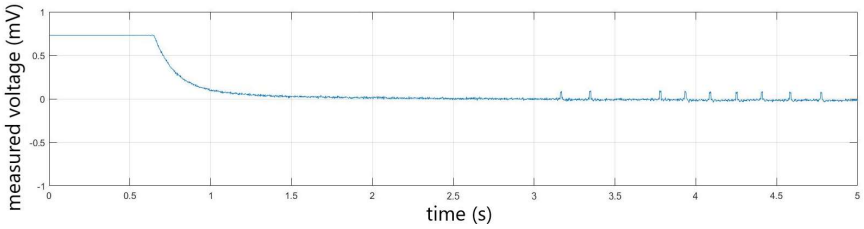

Figure 54: Rejection effect of the high-pass-filter on the DC offset introduced by the SMU.

The pulse amplitude required was tens of µV to emulate the real spike shape. In this session, trains of positive pulses with 50 µV amplitude and 1 ms width were generated from the SMU to assess the board's capability to correctly detect the peaks. The outcomes are displayed in **Figure 55**.

Finally, one of the detected pulses has been compared to a real neuronal spike recorded by the USB-MEA60-Inv-BC-System, to give a visual representation of the similarity between the two systems in terms of performance. The two peaks have been superimposed in **Figure 56**.

This first phase of tests demonstrated the abilities of the board under simulated conditions. The next steps involved proving the reproducibility of the results on real cell cultures and conducting experiments for the research.

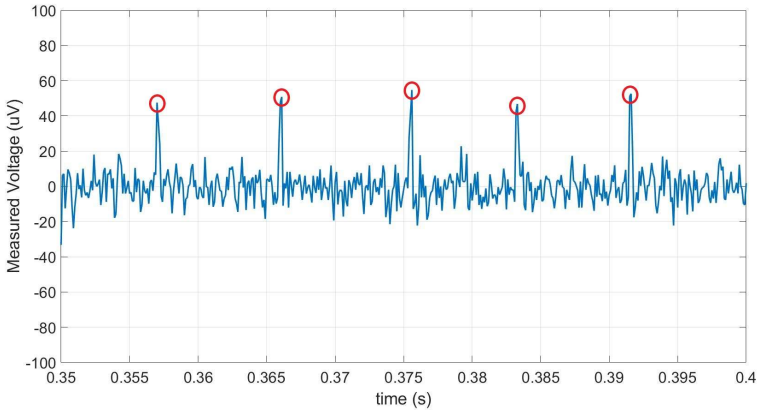

Figure 55: Recording under simulated conditions. Red circles indicate the peaks of the detected 50 µV pulses generated by the SMU.

3.2 Cell Culture Recordings

After the device was assembled with the MEA within the incubator, it was turned on and began taking measurements. By looking at the tracks of the 60 channels obtained with the USB-MEA60-Inv-BC-System, five channels were selected:

- Channel 61
- Channel 51
- Channel 54
- Channel 66
- Channel 62

The first (ch. 61) has been selected to evaluate the noise, due to the lack of neuron electrical activity in proximity to the correspondent electrode. **Figure 57** displays the signal recorded by the AFE board.

It is clear that the noise is contained within ± 10 μV_{pp}. The RMS noise value (calculated with the equation 3.2) is:

$$V_{RMS,Ch61} = 3.3\mu V \tag{3.3}$$

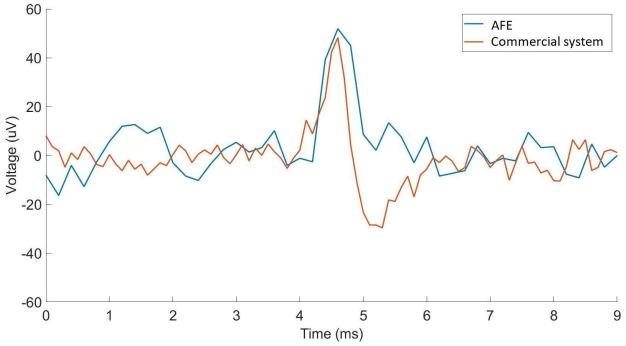

Figure 56: Simulated spike recording with AFE (blue) VS real spike recording with the commercial acquisition system (red).

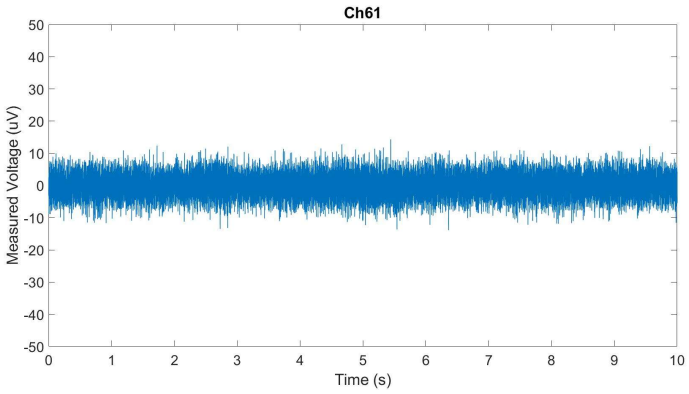

Figure 57: AFE recording from Channel 61, chosen for its inactivity.

This value is lower than the 5.1 μV_{RMS} noise calculated under simulated conditions. This may be caused by the better insulation of the system inside the incubator from external interference sources, than the small Faraday cage used at DET. The short path between the MEA's pad and the AFE's input could also have improved performance during the cell culture tests, in comparison with the simulations, where relatively long jump-wires were used for connecting the water to the inputs.

After having evaluated the performance in an inactive electrode, the channels which showed the largest activity during the USB-MEA60-Inv-BC-System acquisitions were registered. The recordings obtained from channels 51, 54 and 66 displayed similar behaviours in terms of performance, ampli-

tude of the neuronal spikes and firing frequency.

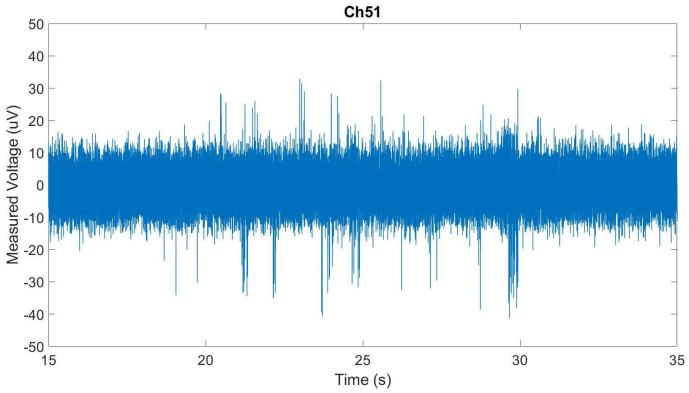

Figure 58: AFE recording from Channel 51.

For channel 51 (**Figure 58**), the performance resulted in being similar in terms of noise amplitude to the inactive channel 61: the peak-to-peak value of the noise is within the range of ±15 µV.

The neuronal spikes are represented either by a uni-phase, mostly with negative peaks, or a bi-phase shape. For this experiment, the spike amplitude and the firing frequency have been calculated in consideration of the negative peaks for both these different shapes. The peak of the spikes was detected by implementing a threshold, which was dependent on the noise level and a minimum distance between two different peaks.

Channel 51's recording showed neuron electrical activity along the whole track. The mean firing frequency and the average spike amplitude were calculated, resulting in:

$$f_{m,Ch51} = 4.4Hz \tag{3.4}$$

$$V_{ap,Ch51} = -23.2\mu V \tag{3.5}$$

The signal from the channel 54 is displayed in **Figure 59**. Also in this case, the performance was evaluated in base of the noise level. As with the previous track analysed, the noise amplitude is contained between ±15 µV. From the detected spikes, the mean firing frequency and the average amplitude were calculated:

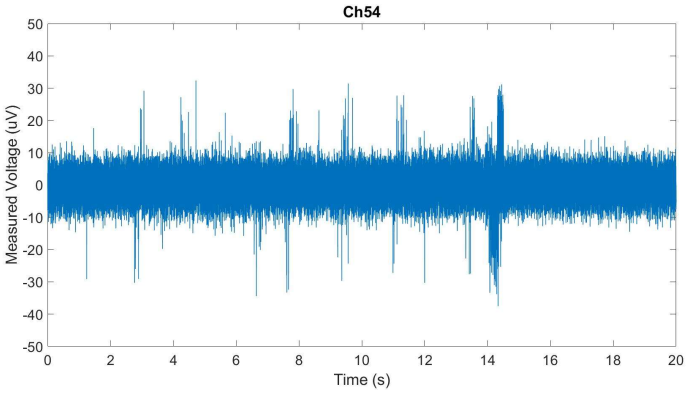

Figure 59: AFE recording from Channel 54.

$$f_{m,Ch54} = 3.6Hz \tag{3.6}$$

$$V_{ap,Ch54} = -22.9\mu V \tag{3.7}$$

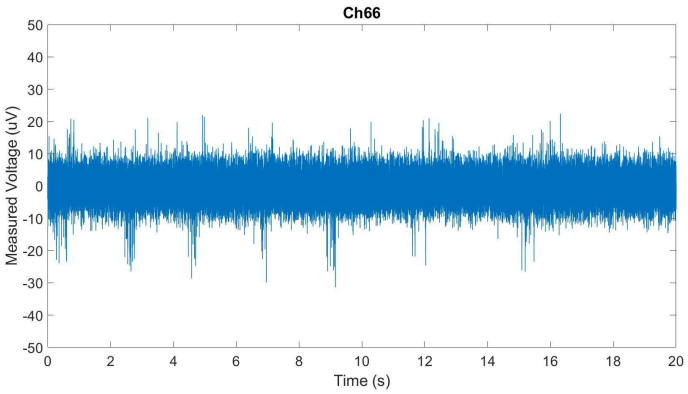

Figure 60: AFE recording from Channel 66.

The same process has been performed for channel 66 (**Figure 60**). The background noise is comparable with the previous channels. Spikes have been detected, resulting in a similar average amplitude and a noticeably lower mean firing frequency:

$$f_{m,Ch66} = 1.0Hz \tag{3.8}$$

$$V_{ap,Ch66} = -22.3\mu V \tag{3.9}$$

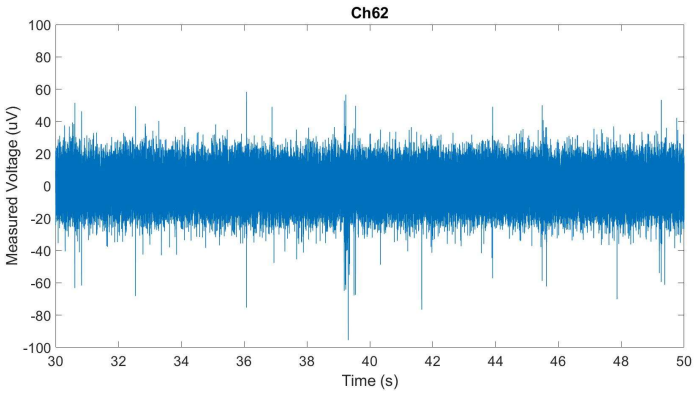

Figure 61: AFE recording from Channel 62.

Finally, channel 62 has been recorded and analysed (**Figure 61**). The outcomes, both from the USB-MEA60-Inv-BC-System and the AFE acquisitions, showed that around the corresponding electrode the electrical activity of neurons was the highest (among the observed channels).

Moreover, this track was also the noisiest. It is uncertain as to why the performance of the AFE consistently dropped when recording on this channel. However, the root-mean square of the noise amplitude, calculated in a non-active section of the signal, was around 9.2 μV_{RMS}, which is still marginally lower than the 10 μV_{RMS} threshold fixed before the tests.

When calculating the mean firing frequency and the average spike amplitude, the following values were obtained:

$$f_{m,Ch62} = 10.6Hz \tag{3.10}$$

$$V_{ap,Ch62} = -37.4\mu V \tag{3.11}$$

Figure 62 displays a zoomed view of a fraction of the track. In this case, two bi-phase spikes, which are part of the same neuron firing burst, are represented.

The power spectral density was estimated with Welch's method, to evaluate the signal in the frequency-domain (**Figure 63**). The PSD is comparable with that obtained from the tests under simulated conditions (**Figure 52**). The contribution of high-frequency components are progressively attenuated

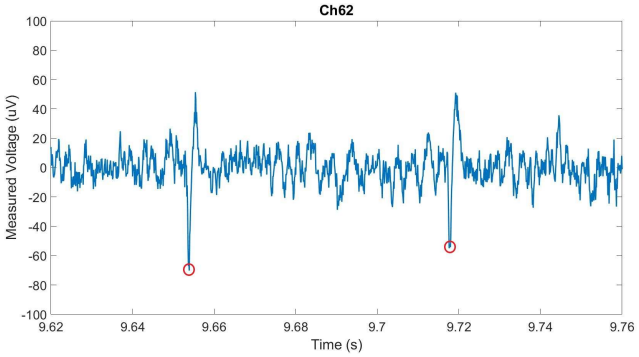

Figure 62: Zoomed spikes from channel 62 recording. The negative peak of each spike is marked with a red circle.

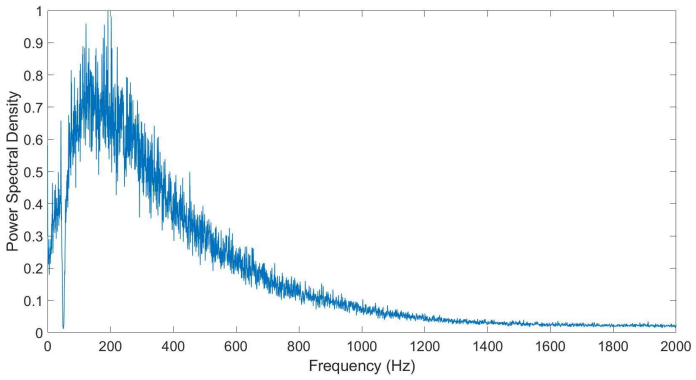

Figure 63: Power spectral density of the channel 62 recording.

by the two active low-pass-filters of the AFE conditioning chain. The 50 Hz rejection is visible on the PSD graph.

The results from channel 62 have been compared with the USB-MEA60-Inv-BC-System acquisitions. For channel 62 the noise results were noticeably higher on the AFE recordings. The spikes had a higher amplitude, as well as a higher firing frequency.

These differences may be due to the fact that the recordings were performed at different times. Indeed, the USB-MEA60-Inv-BC-System acquisitions were taken around 10 minutes earlier than those conducted with the AFE on this specific channel. During this time frame, it is likely that the neuronal network in proximity to the electrode increased its activity and

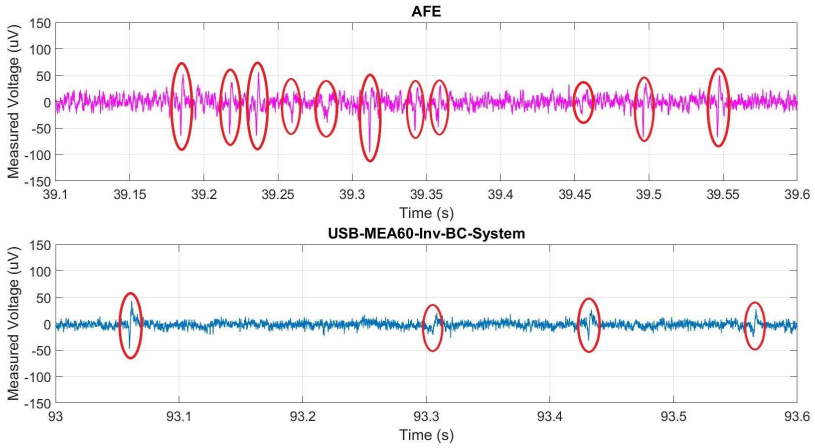

Figure 64: Comparison between AFE recording and USB-MEA60-Inv-BC-System recording, both performed on the same channel (62) at different times (non-simultaneously). The spikes are marked with a red oval.

consequently, the spike parameters changed.

Figure 64 shows the differences between the two acquisitions.

Despite this, the performance of the other channels using the AFE was similar, or better when compared to the commercial system.

3.3 Cell Culture Recordings - Interdigitated Electrodes

In summary, the procedure for this testing session involved two different methods of administration of the glutamate: a massed treatment with a single pulse of 200 µM glutamate, able to saturate the neurons' receptors and a spaced treatment with 5 pulses of 50 µM glutamate.

First, the signal coming from still untreated wells was recorded, to compare with the treated ones. The basal A1 well recording is reported in **Figure 65**.

As expected, no electrical activity was revealed due to the large number of neurons on the interdigitated electrodes.

The massed treatment has been performed on 6 different wells during the acquisition of data, to evaluate the overall response from neurons. **Figure 66** displays the comparison between the massed treatment recording from the A1 well and the basal recording. The A1 well was massed treated again for comparison with the first injection.

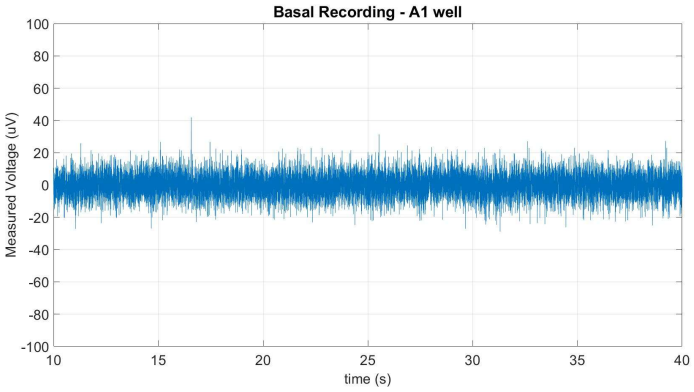

Figure 65: Recording from non-treated A1 well.

As depicted in the graph, when the 200 µM glutamate was administered to the solution the signal moved from the baseline with a sharp wave and returned to a stable condition after about 10 seconds.

When the second treatment was performed, the wave generated from the injection of the neurotransmitter resulted in being much smaller and shorter than the first one.

The final 6 wells were treated with five pulses of 40 µM glutamate each. **Figure 67** reports the recording from the A4 channel under these conditions. The first wave generated by the administration of the initial shot of neurotransmitter produced a similar shape to the massed treatment and was slightly lower in amplitude. By injecting further doses of glutamate, the wave generated became progressively lower in amplitude and the baseline was restored more quickly. The fifth wave was barely detectable from the background noise.

These tests, performed by interfacing the AFE with interdigitated electrodes, had interesting outcomes. However, this session was intended as a pilot experiment in order to understand whether the crossover between the two projects could have been possible. The actual reason these types of results were obtained is unclear: to demonstrate that the waves generated after administering glutamate derived from an overall response by neurons, further tests and analysis need to be conducted in the future.

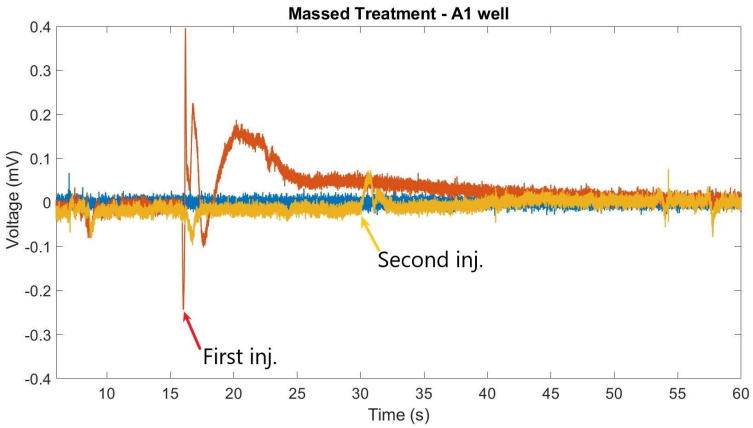

Figure 66: A1 well recordings. In red, the first massed treatment with 200 µM glutamate. The moment of administration is indicated by a red arrow. In blue, the basal recording displays untreated well recording. In yellow, the second massed treatment, also with 200 µM glutamate. The moment of administration is indicated by a yellow arrow.

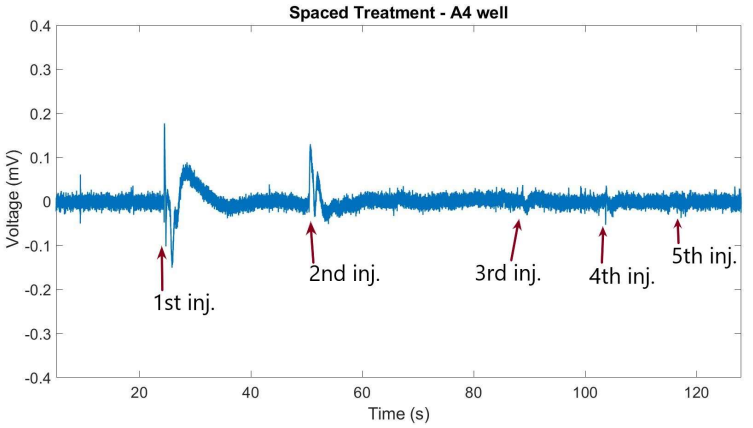

Figure 67: Spaced treatment recording on the A4 well. Red arrows indicate the moments when the 40 µM glutamate was administrated into the solutions.

4 Conclusions

This thesis dissertation proposed the design and development of an early-stage readout device for cultured cells, planted on innovative micro-electrodes. The primary purpose was to obtain a cheap and versatile acquisition system, able to provide the user with low-noise and reliable potentiometric recordings to detect the neuronal electrical activity coming from a cell culture.

The device has been tested under different conditions in order to evaluate its performance and to conduct experiments for neuroscientific research. First, the electrical activity of neurons was simulated, by generating pulses from a precision source-measure unit and recorded with the customized system. This ensured the possibility of performing intensive sessions of tests, without waiting for the cultured cells to mature. Hence, real cell cultures have been tested in potentiometric mode. Finally, the analog front-end was used as an acquisition system for recordings from cultured neurons plated on interdigitated electrodes.

The analog front-end demonstrated good performances under all the conditions. The goal of having a root-mean-square noise amplitude lower than 10 µV has been reached, achieving the possibility to conduct physiological analysis on neurons.

The results obtained during the implementation of this work were promising, advocating the plans to continue this as an ambitious project.

Further developments of the device, beyond the improvement of its current performance, include the expansion to 60 independent channels. In doing so, parallel and simultaneous recordings from the whole cell culture would be possible. This would be advantageous for studying the information processing and learning aspects of the neuronal network behaviour. Including a stimulation/measurement modality is another possibility to increase the number of tasks the device might be able to perform.

Moreover, one of the key goals for future implementations involve designing additional circuits for performing simultaneous acquisitions with different electrochemical methods, such as amperometry. This may prove extremely useful for research into certain neurodegenerative pathologies, such as Parkinson's Disease.

References

[1] "Neurological disorders affect millions globally: Who report." https://www.who.int, 02 2007.

[2] D. M. Ecker and P. Seymour, "Forecasts for biomanufacturing capacity." https://bioprocessintl.com/business/economics/forecasts-for-biomanufacturing-capacity, 02 2020.

[3] M. E. J. Obien, K. Deligkaris, T. Bullmann, D. J. Bakkum, and U. Frey, "Revealing neuronal function through microelectrode array recordings," *Frontiers in Neuroscience*, vol. 8, 2015.

[4] "Slideshow: Visual guide to your nervous system." https://www.webmd.com/brain/ss/slideshow-nervous-system-overview, 2017.

[5] "Introduction to the nervous system — seer training." https://training.seer.cancer.gov/anatomy/nervous.

[6] C. L. Stanfield, *Fisiologia*. Edises, 04 2012.

[7] T. Newman, "Neurons: What are they and how do they work?." https://www.medicalnewstoday.com/articles/320289, 12 2017.

[8] F. A. Azevedo, L. R. Carvalho, L. T. Grinberg, J. M. Farfel, R. E. Ferretti, R. E. Leite, W. J. Filho, R. Lent, and S. Herculano-Houzel, "Equal numbers of neuronal and nonneuronal cells make the human brain an isometrically scaled-up primate brain," *The Journal of Comparative Neurology*, vol. 513, pp. 532–541, 04 2009.

[9] J. Hawkins and S. Ahmad, "Why neurons have thousands of synapses, a theory of sequence memory in neocortex," *Frontiers in Neural Circuits*, vol. 10, 2016.

[10] "Organization of the nervous system." https://content.byui.edu, 2013.

[11] A. Fletcher, "Action potential: Generation and propagation," *Anaesthesia and Intensive Care Medicine*, vol. 20, pp. 243–247, 04 2019.

[12] E. Olivi, *Coupling of numerical methods for the forward problem in Magneto- and Electro-Encephalography. Numerical Analysis [cs.N A]*. Theses, Université Nice Sophia Antipolis, 12 2011.

[13] "A.3.5. saltatory propagation." http://basicphysiology.com, 2017.

[14] A. E. Pereda, "Electrical synapses and their functional interactions with chemical synapses," *Nature Reviews Neuroscience*, vol. 15, pp. 250–263, 03 2014.

[15] S. E. Hyman, "Neurotransmitters," *Current Biology*, vol. 15, pp. R154–R158, 03 2005.

[16] H. Juárez Olguín, D. Calderón Guzmán, E. Hernández García, and G. Barragán Mejía, "The role of dopamine and its dysfunction as a consequence of oxidative stress," *Oxidative Medicine and Cellular Longevity*, vol. 2016, pp. 1–13, 2016.

[17] G. Tomagra, F. Picollo, A. Battiato, B. Picconi, S. De Marchis, A. Pasquarelli, P. Olivero, A. Marcantoni, P. Calabresi, E. Carbone, and V. Carabelli, "Quantal release of dopamine and action potential firing detected in midbrain neurons by multifunctional diamond-based microarrays," *Frontiers in Neuroscience*, vol. 13, 2019.

[18] S. J. Chinta and J. K. Andersen, "Dopaminergic neurons," *The International Journal of Biochemistry and Cell Biology*, vol. 37, pp. 942–946, 05 2005.

[19] M. A. Ungless, "Uniform inhibition of dopamine neurons in the ventral tegmental area by aversive stimuli," *Science*, vol. 303, pp. 2040–2042, 03 2004.

[20] A. Fiorenzano, E. Sozzi, M. Parmar, and P. Storm, "Dopamine neuron diversity: Recent advances and current challenges in human stem cell models and single cell sequencing," *Cells*, vol. 10, no. 6, 2021.

[21] W. Contributors, "Substantia nigra." https://en.wikipedia.org/wiki/Substantia_nigra, 03 2019.

[22] W. Contributors, "Striatum." https://en.wikipedia.org/wiki/Striatum, 2019.

[23] T. M. Axelsen and D. P. Woldbye, "Gene therapy for parkinson's disease, an update," *Journal of Parkinson's Disease*, vol. 8, pp. 195–215, 06 2018.

[24] C.-P. Segeritz and L. Vallier, "Cell culture: Growing cells as model systems in vitro," *Basic Science Methods for Clinical Researchers*, pp. 151–172, 2017.

[25] C. Suñol, Z. Babot, E. Fonfría, M. Galofré, D. García, N. Herrera, S. Iraola, and I. Vendrell, "Studies with neuronal cells: From basic studies of mechanisms of neurotoxicity to the prediction of chemical toxicity," *Toxicology in Vitro*, vol. 22, no. 5, pp. 1350–1355, 2008. Proceedings of the Scandinavian Society of Cell Toxicology 2007 Workshop.

[26] M.-T. Arango, P. Quintero-Ronderos, J. Castiblanco, and G. Montoya-Ortíz, *Cell Culture and Cell Analysis*, ch. 45. Autoimmunity: from Bench to Bedside [Internet], El Rosario University Press, 07 2013.

[27] A. Verma, M. Verma, and A. Singh, "Animal tissue culture principles and applications," *Animal Biotechnology*, p. 269–293, 2020.

[28] M. E. Spira and A. Hai, "Multi-electrode array technologies for neuroscience and cardiology," *Nature Nanotechnology*, vol. 8, pp. 83–94, 02 2013.

[29] J. Pas, *Flexible neural probes with a fast bioresorbable shuttle : From in vitro to in vivo electrophysiological recordings*. PhD thesis, Université de Lyon, 12 2017.

[30] "Mea2100-systems, the newest multi electrode array." `https://nbtltd.com/products/mea2100-systems/`.

[31] C. M. A. Brett and A. Maria, *Electrochemistry : Principles, Methods, and Applications*. Oxford University Press, 2005.

[32] Wikipedia contributors, "Galvanic cell." `https://en.wikipedia.org/wiki/Galvanic_cell`, 11 2019.

[33] S. Lower, "Galvanic cells and electrodes." `https://chem.libretexts.org/Bookshelves/General_Chemistry/`, 03 2022.

[34] V. S. Bagotsky, *Fundamentals of Electrochemistry*. Wiley-Interscience, 2nd ed., 2006.

[35] Wikipedia contributors, "Electroanalytical methods." `https://en.wikipedia.org/w/index.php?title=Electroanalytical_methods&oldid=1074452309`, 2019.

[36] R. L. Gil, C. G. Amorim, M. C. B. S. M. Montenegro, and A. N. Araújo, "Potentiometric detection in liquid chromatographic systems: an overview," *Journal of Chromatography A*, vol. 1602, p. 326–340, 09 2019.

[37] S. Grimnes and Ørjan G Martinsen, "Chapter 7 - electrodes," in *Bioimpedance and Bioelectricity Basics (Third Edition)* (S. Grimnes and Ørjan G Martinsen, eds.), pp. 179–254, Oxford: Academic Press, third edition ed., 2015.

[38] E. S. Bucher and R. M. Wightman, "Electrochemical analysis of neurotransmitters," *Annual Review of Analytical Chemistry (Palo Alto, Calif.)*, vol. 8, p. 239–261, 2015.

[39] A. Peroff, "What is a potentiostat and how does it work?." `https://pineresearch.com/shop/kb/theory/instrumentation/what-potentiostat-does/`, 04 2021.

[40] X. Liu, Y. Tong, and P.-P. Fang, "Recent development in amperometric measurements of vesicular exocytosis," *TrAC Trends in Analytical Chemistry*, vol. 113, pp. 13–24, 2019.

[41] A. Gladkov, Y. Pigareva, D. Kutyina, V. Kolpakov, A. Bukatin, I. Mukhina, V. Kazantsev, and A. Pimashkin, "Design of cultured neuron networks in vitro with predefined connectivity using asymmetric microfluidic channels," *Scientific Reports*, vol. 7, p. 15625, 11 2017.

[42] K. H. Pettersen and G. T. Einevoll, "Amplitude variability and extracellular low-pass filtering of neuronal spikes," *Biophysical Journal*, vol. 94, pp. 784–802, 02 2008.

[43] K. Okamoto, T. Ishikawa, R. Abe, D. Ishikawa, C. Kobayashi, M. Mizunuma, H. Norimoto, N. Matsuki, and Y. Ikegaya, "Ex vivo cultured neuronal networks emit in vivo-like spontaneous activity," *The journal of physiological sciences : JPS*, vol. 64, 09 2014.

[44] B. O. Watson, D. Levenstein, J. P. Greene, J. N. Gelinas, and G. Buzsáki, "Network homeostasis and state dynamics of neocortical sleep," *Neuron*, vol. 90, pp. 839–852, 05 2016.

[45] K. Mizuseki and G. Buzsáki, "Preconfigured, skewed distribution of firing rates in the hippocampus and entorhinal cortex," *Cell Reports*, vol. 4, pp. 1010–1021, 09 2013.

[46] A. Mazzoni, F. D. Broccard, E. Garcia-Perez, P. Bonifazi, M. E. Ruaro, and V. Torre, "On the dynamics of the spontaneous activity in neuronal networks," *PLOS ONE*, vol. 2, pp. 1–12, 05 2007.

[47] L. J. Mellander, R. Trouillon, M. I. Svensson, and A. G. Ewing, "Amperometric post spike feet reveal most exocytosis is via extended kiss-and-run fusion," *Scientific Reports*, vol. 2, 11 2012.

[48] K. D. Gillis, X. A. Liu, A. Marcantoni, and V. Carabelli, "Electrochemical measurement of quantal exocytosis using microchips," *Pflügers Archiv - European Journal of Physiology*, vol. 470, pp. 97–112, 09 2017.

[49] T. Moser and E. Neher, "Estimation of mean exocytic vesicle capacitance in mouse adrenal chromaffin cells," *Proceedings of the National Academy of Sciences*, vol. 94, no. 13, pp. 6735–6740, 1997.

[50] F. Picollo, A. Battiato, E. Bernardi, A. Marcantoni, A. Pasquarelli, E. Carbone, P. Olivero, and V. Carabelli, "Microelectrode arrays of diamond-insulated graphitic channels for real-time detection of exocytotic events from cultured chromaffin cells and slices of adrenal glands," *Analytical Chemistry*, vol. 88, pp. 7493–7499, 07 2016.

[51] G. Tomagra, C. Franchino, A. Pasquarelli, E. Carbone, P. Olivero, V. Carabelli, and F. Picollo, "Simultaneous multisite detection of quantal release from pc12 cells using micro graphitic-diamond multi electrode arrays," *Biophysical Chemistry*, vol. 253, p. 106241, 10 2019.

[52] G. Regalia, E. Biffi, G. Ferrigno, and A. Pedrocchi, "A low-noise, modular, and versatile analog front-end intended for processing¡i¿in vitro¡/i¿neuronal signals detected by microelectrode arrays," *Computational Intelligence and Neuroscience*, vol. 2015, pp. 1–15, 2015.

[53] "Decoupling capacitor." `https://en.m.wikipedia.org/wiki/Decoupling_capacitor`, 06 2022.

[54] G. Kaur, A. Q. Ansari, and M. S. Hashmi, "Third order sallen key lowpass filter in fractional domain," in *2018 International Conference on Computing, Power and Communication Technologies (GUCON)*, pp. 508–511, 2018.

[55] B. Aremo, M. Oyebamiji Adeoye, I. B. Obioh, and O. A. Adeboye, "A simplified microcontroller based potentiostat for low-resource applications," *Open Journal of Metal*, vol. 05, pp. 37–46, 2015.

[56] F. Picollo, A. Battiato, E. Carbone, L. Croin, E. Enrico, J. Forneris, S. Gosso, P. Olivero, A. Pasquarelli, and V. Carabelli, "Development and characterization of a diamond-insulated graphitic multi electrode

array realized with ion beam lithography," *Sensors*, vol. 15, no. 1, pp. 515–528, 2015.

[57] B. Kuhn, F. Picollo, V. Carabelli, and G. Rispoli, "Advanced real-time recordings of neuronal activity with tailored patch pipettes, diamond multi-electrode arrays and electrochromic voltage-sensitive dyes," *Pflügers Archiv - European Journal of Physiology*, vol. 473, pp. 15–36, 10 2020.

[58] J. Pruszak, L. Just, O. Isacson, and G. Nikkhah, "Isolation and culture of ventral mesencephalic precursor cells and dopaminergic neurons from rodent brains," *Current Protocols in Stem Cell Biology*, vol. 11, 12 2009.